Fall 2013

Part height control of laser metal additive manufacturing process

Yu-Herng Pan

Department:

PART HEIGHT CONTROL OF

LASER METAL ADDITIVE MANUFACTURING PROCESS

by

YU-HERNG PAN

A THESIS

Presented to the Faculty of the Graduate School of the

MISSOURI UNIVERSITY OF SCIENCE AND TECHNOLOGY

In Partial Fulfillment of the Requirements for the Degree

MASTER OF SCIENCE IN MANUFACTURING ENGINEERING

2013

Approved by

Dr. Frank Liou, Advisor
Dr. Edward C. Kinzel
Dr. Joseph W. Newkirk

ABSTRACT

Laser Metal Deposition (LMD) has been used to not only make but also repair damaged parts in a layer-by-layer fashion. Parts made in this manner may produce less waste than those made through conventional machining processes. However, a common issue of LMD involves controlling the deposition's layer thickness. Accuracy is important, and as it increases, both the time required to produce the part and the material wasted during the material removal process (e.g., milling, lathe) decrease. The deposition rate is affected by multiple parameters, such as the powder feed rate, laser input power, axis feed rate, material type, and part design, the values of each of which may change during the LMD process. Using a mathematical model to build a generic equation that predicts the deposition's layer thickness is difficult due to these complex parameters. In this thesis, we propose a simple method that utilizes a single device. This device uses a pyrometer to monitor the current build height, thereby allowing the layer thickness to be controlled during the LMD process. This method also helps the LMD system to build parts even with complex parameters and to increase material efficiency.

ACKNOWLEDGMENTS

This work could not have been completed without the support I received from a number of people. First, I would like to express my sincere appreciation to my advisor, Dr. Frank Liou, for accepting me into the lab. Dr. Liou also served as a constant source of encouragement throughout my research. I am grateful to Mr. Todd Sparks for both his scholarly guidance and his friendship. I must also thank the Manufacturing Engineering Department for the research assistantship offered to me.

I would like to thank my committee members, Dr. Joseph W. Newkirk and Edward C. Kinzel, for both the time and advice they offered during this research. I sincerely thank the LAMP lab members for the friendly atmosphere they helped to create and the suggestions they offered when I was struggling. I am also grateful for all of my friends in Rolla, Missouri. They helped me create unforgettable memories throughout the past two years.

Finally, I would like to express my gratitude to both of my parents, Mr. Ci-Ling Pan and Mrs. Ru-Pin Chao, and my brother, Yu-Chin Pan, for their unconditional love and support.

TABLE OF CONTENTS

Page

LIST OF ILLUSTRATIONS

Page

LIST OF TABLES

Page

1. INTRODUCTION

1.1 OVERVIEW

Laser Metal Deposition (LMD) is now widely pursued as an advanced manufacturing technology. It has several advantages over conventional metal manufacturing processes, including casting, rolling, forging, machining, and welding. Because it is an additive metal manufacturing process, the LMD process can repair damaged, expensive, and unique parts. It also can produce parts with unique shapes and complex internal structures at a lower cost than traditional metal manufacturing processes [1]. LMD can build a prototype part or conduct a low-volume run directly from a three-dimensional (3D) Computer Aided Design (CAD) model [2]. A wide variety of materials can be processed this way, from exotic aerospace material (e.g. Titanium), to materials commonly found in many industrial products (e.g., stainless steel and tool steel). The LMD process also can produce both fully dense and net-shaped parts, which other metal additive manufacturing processes cannot accomplish [3].

Because it is an additive metal manufacturing process, LMD builds parts in a layer-by-layer fashion rather than removing materials. In the LMD process, a molten pool of base material is created using a focused, high-power laser beam. A metal bead of melting material forms on the melt pool when material is fed into the melt pool. While the material is being fed, a laser focusing position moves along a designed path. After the laser moves away, a metal bead in the laser's previous position cools down and solidifies. Each finished path represents one layer of the built part. The next layer will be deposited

on top of the previous layer. Continuing this layer-by-layer process according to the design produces a complete, precisely made part.

Controlling the layer thickness is essential to the LMD process. It not only improves the part's geometric precision, but also allows the quantity of the material fed into the melt pool to be optimized. Figure 1.1 illustrates two major nozzle types, concentric and side nozzles, used to feed the powder in the LMD process.

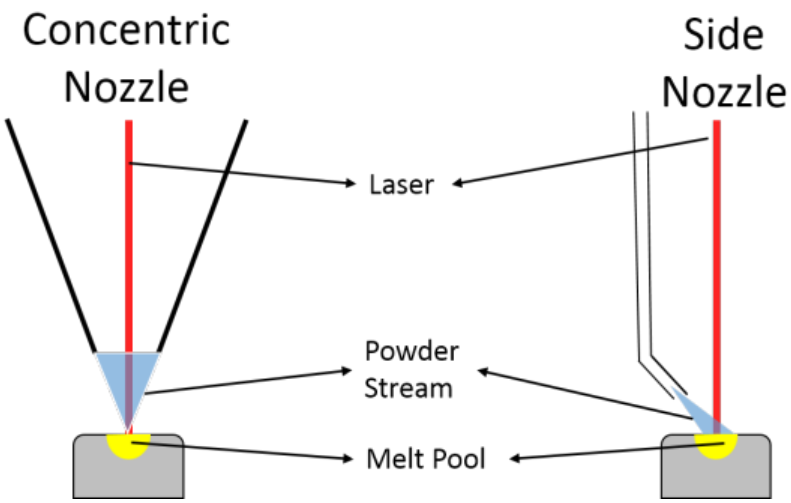

Figure 1.1 Two major types of feed nozzles, the concentric nozzle (left) and the side nozzle (right). Both nozzle types aim powder streams to the melt pool.

The standoff distance in the LMD system is the distance from the powder feeding nozzle to the melt pool. The amount of powder placed into the melt pool of each nozzle type differs by the standoff distance between the feeder edge and the part, as shown in Figure 1.2. Figure 1.3 shows the powder stream from the current feeding nozzle tube. The melt pool receives the most powder at an optimal standoff distance and less when the distance is either too long or too short. If a higher percentage of material is fed into the

system, a smaller amount of time is required to build a complete part, and less material is wasted during the LMD process.

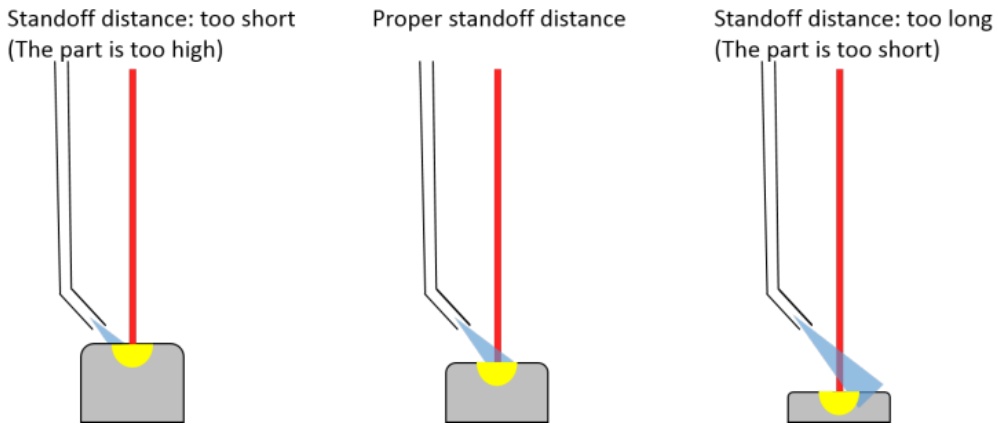

Figure 1.2 Amount of powder fed into the melt pool varies under different standoff distances. The powder stream is not aligned to the melt pool in the cases represented by the right and left figures because of improper standoff distances. The melt pool captures the highest percentage of powder in the case represented by the center figure because the powder stream is aligned to the melt pool.

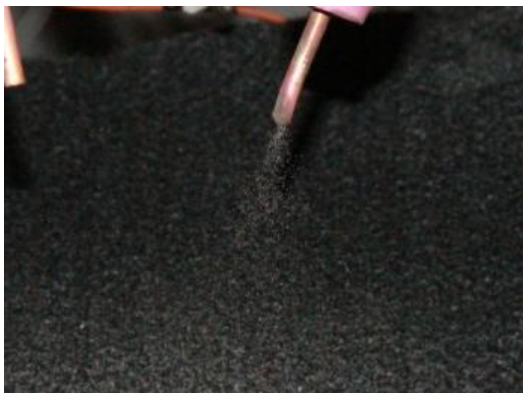

Figure 1.3 Powder stream from current powder feeding tube. The powder stream exits the copper nozzle in the center of the figure. The tube's outer diameter is 0.125".

The most common reason for having a less than optimal standoff distance is an incorrect estimation of the part's layer thickness. An inconsistent powder feed rate also

can cause the part building rate to vary. Without any feedback control, any change in parameters, such as the laser power, powder feeding rate, or machine table speed, will result in layers of different thicknesses.

Furthermore, the speed at which a deposited layer grows on the part depends dynamically on the melt pool size due to the part's thermal properties coming into play during the process [4]. When deposition begins, the substrate is cool, and the melt pool is much smaller than the substrate. More heat is required at this time to maintain the melt pool's size than at any point during the remainder of the process. Additionally, the heat transfer condition also changes according to the part area change and the temperature difference between the melt pool, the part, and the environment throughout the process. A larger part surface area causes higher heat convection. Less difference between the melt pool, the part, and the environment yields lower thermal conduction. Therefore, if every parameter remains constant throughout the entire process, regardless of how precisely each parameter has been chosen, the thickness of each layer may differ.

Both closed-loop and open-loop height control method have been investigated in previous studies. For open-loop control, a powder feed interface can be created by managing both the carrier gas feed and the feeding nozzle tube position [5]. Powders will appear only under the interface; thus, the deposit can build only until the powder reaches the interface. The layer thickness will relate only to the feeder's position and not to other parameters. This method, however, has the potential to waste more powder. The powder will not fall into the melt pool when the part is at the same height or higher than the powder stream. Thus, this method does not build with maximum material efficiency

throughout the process, further increasing the cost. The material efficiency is the ratio of the mass of the final part to the total material mass used during the process.

A sensor for feedback control is required for closed-loop height control system[6-8]. Both cameras and 3D scanners frequently are chosen as feedback sensors. Sensors determine the part's current build height during the building process. The LMD system controller uses this information to adjust parameters, such as laser power, powder feed rate, table axis speed, and others, if necessary. Both cameras and scanners, however, have drawbacks. Cameras can provide high-resolution information regarding part geometry, which requires large files to store each picture frame. These files take longer to transfer between devices, and analyzing the information on the files also takes a long time. Although a 3D scanner data file may be smaller, it typically cannot acquire data when the laser is on due to both high heat and laser light. The 3D scanner also takes longer to acquire data than the camera.

A new feedback control system for height control is introduced in this thesis. A pyrometer, the MIKRON MI-GA 5-LO, was used as a height indicator in the system. It used two wavelengths, 1.45μm and 1.8 μm, to measure the temperature. Measuring the slope of the spectrum radiance on these two wavelengths yielded a temperature determination. The wavelength of the laser used in the LMD system was 1080 nm. Thus, the laser did not affect the pyrometer's reading. Figure 1.4 shows the spectrum radiance according to the wavelength for temperatures of 1660K, 1373K, and 1173K. Figure 1.4 was plotted using Planck's law of black body radiation, which is given in Equation 1.1.1.

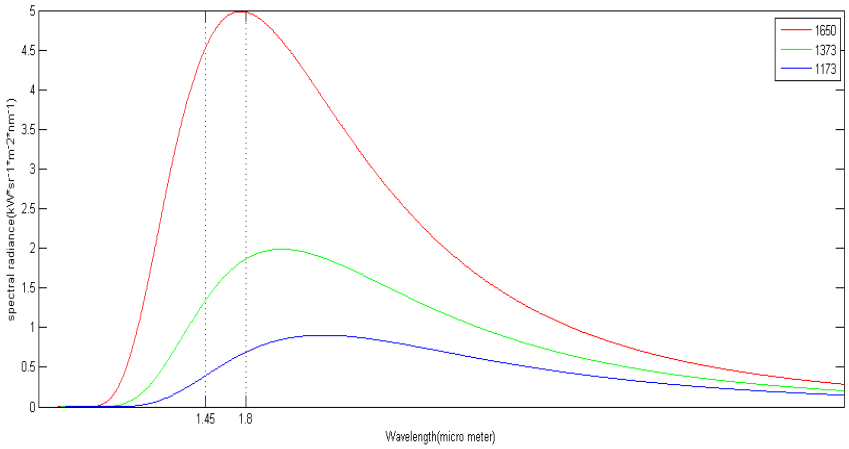

Figure 1.4 Spectrum radiance according to the wavelength for temperatures of 1660K (red line), 1373K (green line) and 1173K (blue line). The pyrometer used wavelengths of 1.45$\boldsymbol{\mu m}$ and 1.8 $\boldsymbol{\mu m}$ to determine the temperature.

$$B_\lambda(\mathrm{T}) = \frac{2hc^2}{\lambda^5}\frac{1}{e^{\frac{hc}{\lambda k_B T}} - 1} \qquad (1.1.1)$$

Where B is the spectral radiance, T is the absolute temperature, k_B is the Boltzmann constant, h is the Planck constant, and c is the speed of light. The pyrometer measuring the area was larger than the melt pool, so any light emitted from the surrounding area would have affected the pyrometer reading. As Figure 1.4 indicates, the spectrum radiance at the melting point of stainless steel 316-L, 1660K, was much higher than at the temperature around the melt pool, approximately 1373K. Therefore, a pyrometer may not be suitable for measuring the temperature around the melt pool, but it appears sufficient for determining the hottest position on the part. The pyrometer acquired its strongest signal at the hottest spot because the area it measured included most of the melt pool.

A laser power management sensor designed specifically for the LMD process by the LAMP lab was used to control power in the height control system. Both sensors operated during the process and output relatively simple signals (when compared to cameras and scanners). A new LMD system was built with both sensors. This new system is based on the previous system built in the LAMP lab at the Missouri University of Science & Technology (MST) [9-10]. Based on the information acquired by the sensors, this new system can control not only the table's speed, but also its position during the process. This capability makes height control possible.

2. THEORY

2.1 POWDER CAPTURING RATE

The alignment of the powder stream greatly affects the rate at which the system captures the material. The material capturing rate is the ratio of the powder mass fed into the part to the total material mass used during the process. This section will include a discussion of the effect of misaligning the powder stream.

Powder stream images were taken to investigate the powder spray angle. When multiple images were merged and the background noise removed, the stream flow became visible and could be analyzed with a computer. Figure 2.1 compares the original image to the image after processing. The whiter spots represent more powder than the darker areas.

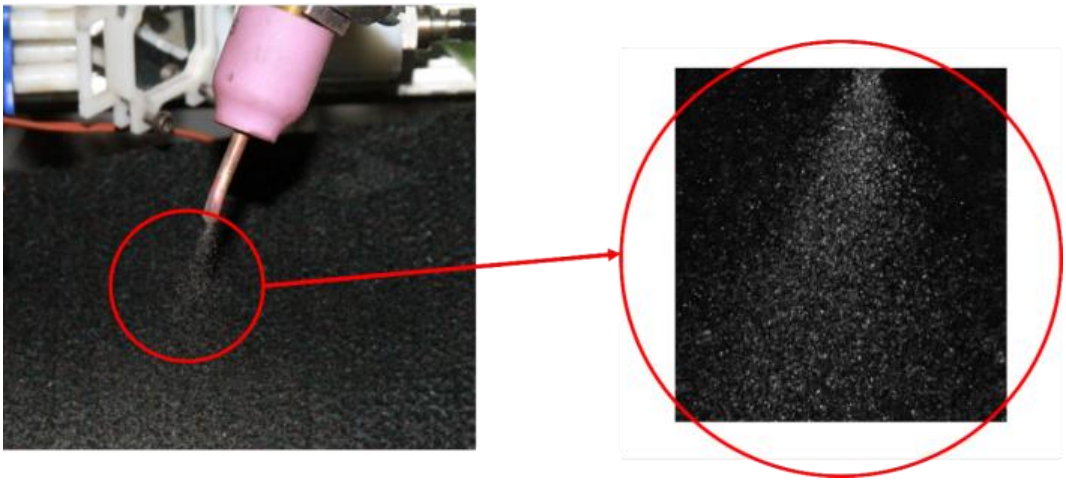

Figure 2.1 Comparison between the original image and the image after processing: The picture on the right is the result of merging multiple pictures into one and removing the background noise.

Figure 2.2 illustrates an example of a result obtained by slicing the powder stream image. A powder distribution chart along the row was plotted by slicing the image row by row. Figure 2.3 shows the normal probability plot of the slicing data in Figure 2.2, which came very close to a normal distribution. The Jarque-Bera test, Kolmogorov-Smirnov test, and Lilliefors test were performed to determine the normality of the slicing data. All three tests indicated that the data were well modeled by a normal distribution curve at a 0.05 significance level. Therefore, the powder stream distribution was considered a normal distribution. The peak value in Figure 2.2 was considered the mean value of the normal distribution. The distance of one standard deviation from the mean position was estimated using Equation 2.1.1

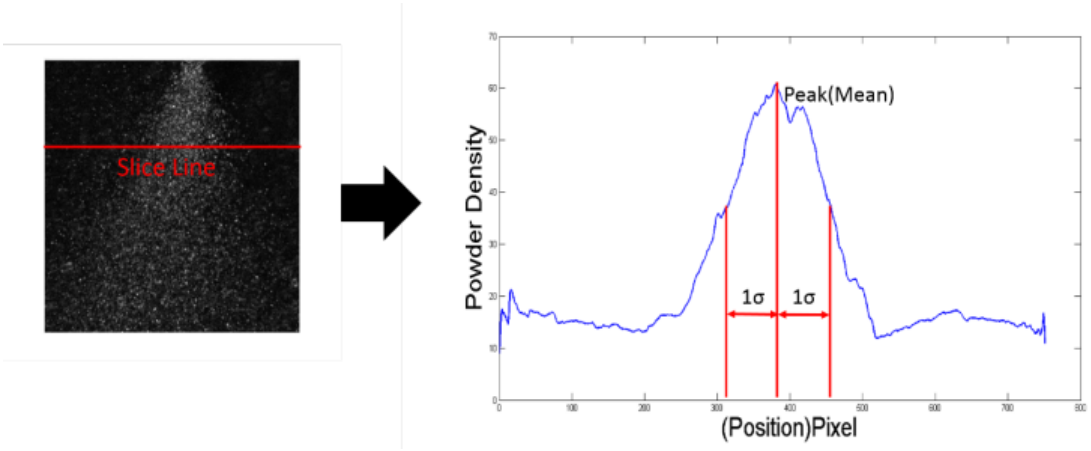

Figure 2.2 Powder stream image slicing: Slicing data plot (right) based on the original powder stream image (left).

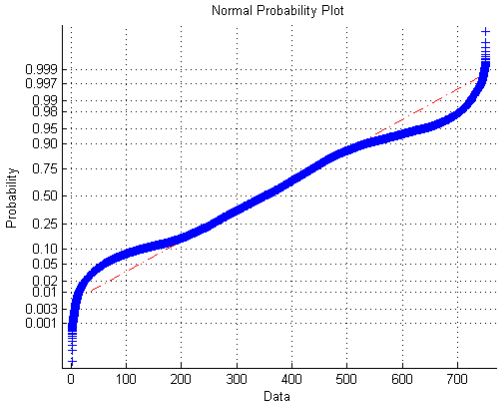

Figure 2.3 Powder distribution normal probability plot: Blue line represents powder stream plot, and red line represents normal distribution plot.

$$D_p \big/ D_\sigma = P_M \big/ P_\sigma \qquad (2.1.1)$$

Where D_p is the peak powder density, D_σ is the powder density at the one sigma position, P_M is the probability at the mean position of the normal distribution, and P_σ is the probability at the one sigma position of the normal distribution. Using Equation 2.1 to find the D_σ, the one sigma position is the position that has the D_σ value on the slicing plot in Figure 2.2.

The angle of the powder stream spread containing 68% of the powder (one sigma in both regions) was calculated by collecting the one standard deviation position along the image's pixel rows and then making regression lines according to those points. The angle was 7.1 degrees. Figure 2.4 illustrates both the regress line and the powder stream's spray angle.

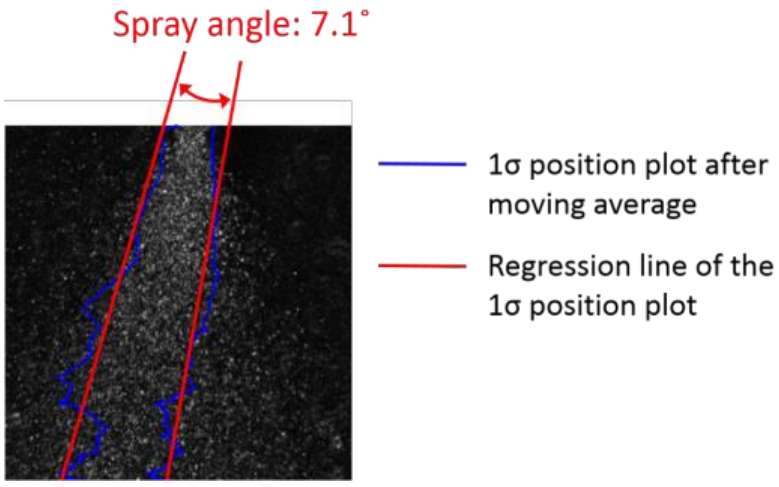

Figure 2.4 Powder stream spread angle: The area between the red lines represents the area containing 68% of the powder.

The projecting area on the melt pool was assumed to be an ellipse, as shown in Figure 2.5.

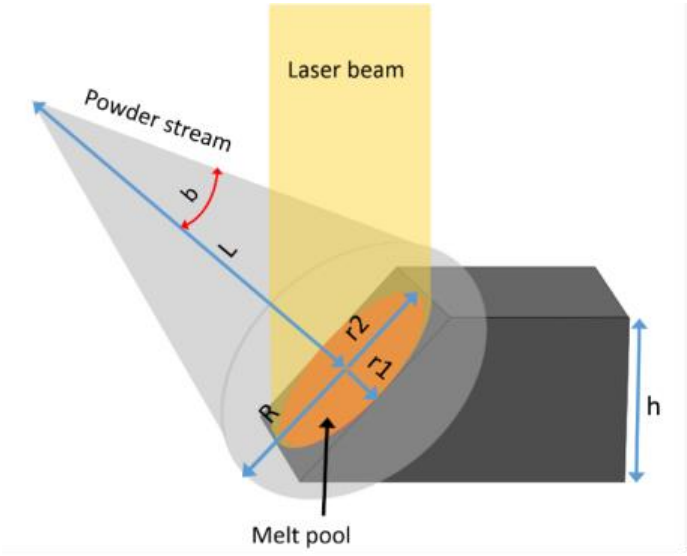

Figure 2.5 Powder flow projection area on the melt pool: The melt pool's shape on the part was assumed to be an ellipse. The size of the ellipse was determined by the layer thickness, h, and laser beam diameter, D.

In Figure 2.5, *h* represents the thickness of the deposited layer, *R* is the powder stream cone radius, and *L* is the distance from the powder feed nozzle to the melt pool. Both *r1* and *r2* represent the radius of the melt pool ellipse. Assuming a melt pool width equal to the laser beam's size, *r1* equals half of the beam diameter, 0.4*mm*. If the layer thickness is 0.2*mm*, r2 can be calculated using Equation 2.1.2.

$$2 \cdot r2 \quad = \sqrt{(2 \cdot r1)^2 + (h)^2} \tag{2.1.2}$$

Thus, r2 equals 0.4123*mm*. The distance from the feed nozzle to the melt pool (L) was approximately 10 mm. Therefore, one sigma radius of the powder stream cone was calculated by the spray angle (b) using Equation 2.1.3.

$$R = L \cdot \tan(b)/2 \tag{2.1.3}$$

Because *R* equals 0.6251*mm*, *r1* equals 0.6389σ and *r2* equals 0.6596σ. Because the powder distribution on an area is considered a normal distribution, the percentage of powder distributed on a surface will resemble Figure 2.6.

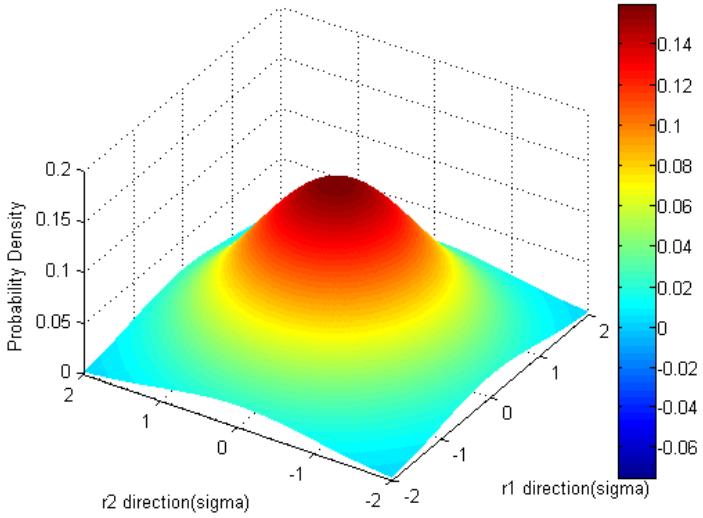

Figure 2.6 Plot of 2d normal distribution. This figure represents the powder distribution of the powder stream on the project surface.

Figure 2.7 illustrates a simulation result of the melt pool powder capturing rate in different cases of powder stream misalignment.

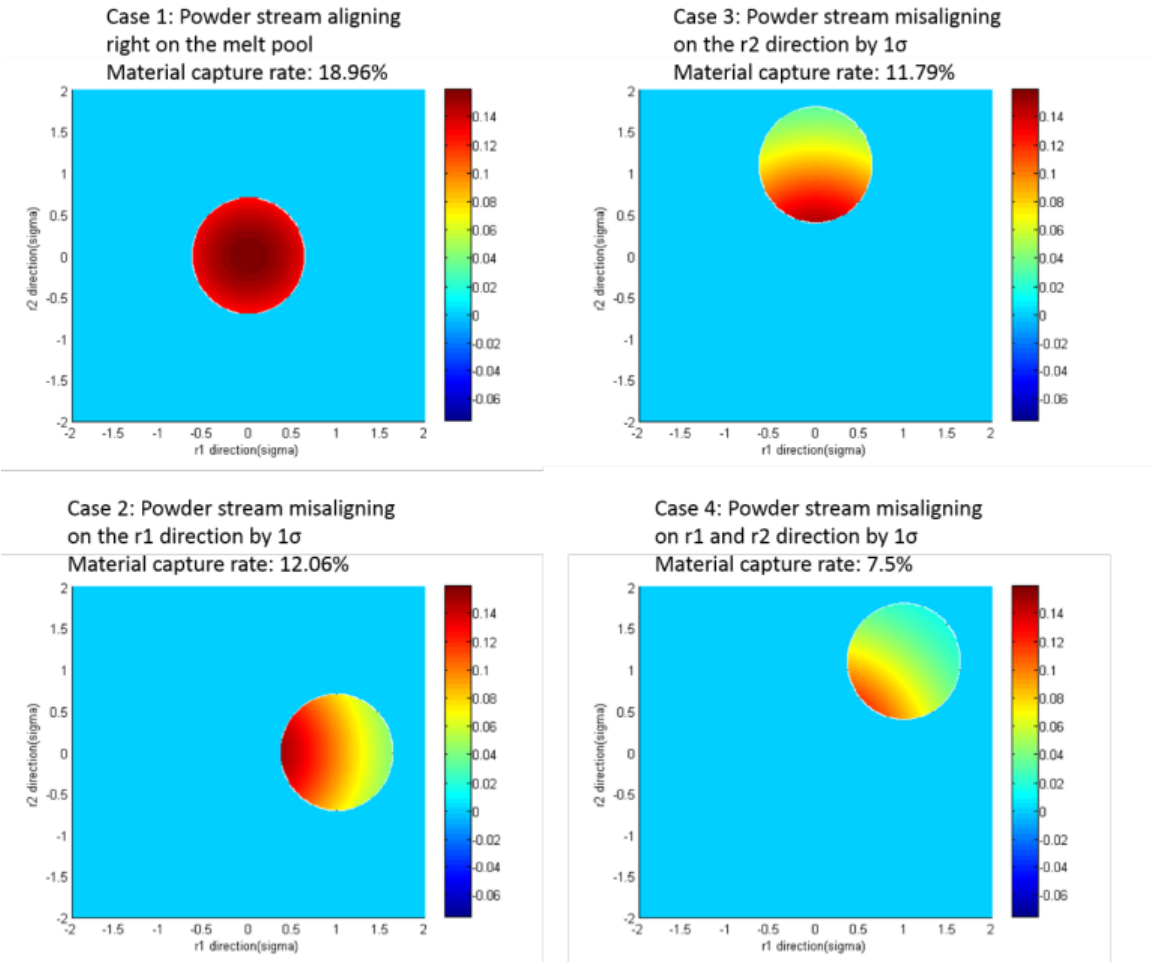

Figure 2.7 Simulation of powder capturing rate in different misalignment cases: In Case 1, the powder stream is aligned on the center of the melt pool. In Case 2, the powder stream is misaligned by one sigma on the r1 direction. In Case 3, the powder stream is misaligned by one sigma on the r2 direction. In Case 4, the powder stream is misaligned by one sigma on both the r1 and r2 directions.

A 1σ (0.6251*mm*) powder stream misalignment on the r1 and r2 directions can cause 60% material loss (compared to Case 1 in Figure 2.7). In contrast, properly aligning the powder stream by maintaining the correct standoff distance can help the LMD system optimize material efficiency.

2.2 SYSTEM RESPONSE TIME

The system response time is critical to the height control system. If the response time is long, the part may be deposited too high during the time between two measurements. Assume that the linear table of the system moves at a speed of *v* to build a certain desired layer thickness *h*. *S* is the distance the table will move for the stepper motor of the linear table to rotate one step. The time required for part S to move is T_s, as defined in Equation 2.2.1:

$$T_s = {}^{S}/_{v} \tag{2.2.1}$$

Therefore, the height build rate $\dot{h}$ can be calculated using Equation 2.2.2:

$$\dot{h} = {}^{h}/_{T_s} \tag{2.2.2}$$

The height error h_ε will be the part build height during the response time T_r.

$$h_\varepsilon = \dot{h} \cdot T_r \tag{2.2.3}$$

$$T_r = {}^{h_\varepsilon}/_{\dot{h}} \tag{2.2.4}$$

S is 0.002 mm in the current system. Assuming a current table speed of 10 mm/s, layer thickness of 0.1 mm, and required height error of less than 0.1 mm, the system

response time must be less than 200 microseconds. This response time is greatly limited by the controller's computing power and the sensor's settling time.

2.3 MAXIMUM TABLE SPEED

For the height control system, the user must set a maximum speed, v_{max}. This is the max speed that the table can move during system operation. The system will slow down the table speed from the max speed according to the height build rate during the process. If the max speed is not high enough, the height control system will fail to maintain the part layer thickness during the process. This behavior can be explained by the volume build rate balancing.

As in Figure 2.8, assume that the minimum part width is the same as the laser beam diameter. The linear table moves the part at speed *v* and builds it with a layer thickness h.

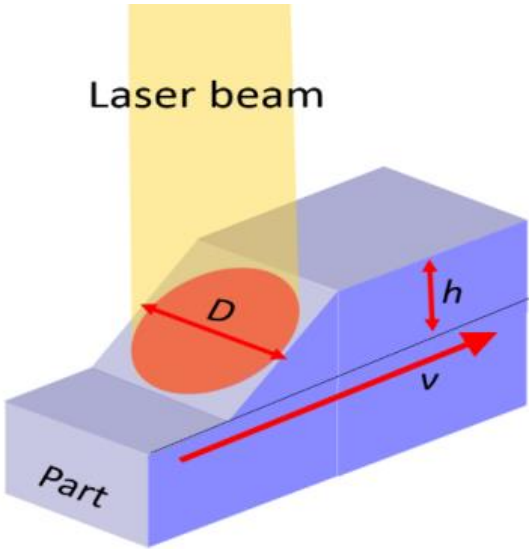

Figure 2.8 Laser with a diameter of D shooting on the part during the LMD process.

When the linear table moves at speed v, the LMD process has a layer thickness of h. Therefore, the volume build rate based on the table speed can be calculated using Equation 2.3.1:

$$\dot{V}_{speed} = v \cdot h \cdot D_{Beam} \tag{2.3.1}$$

The volume build rate also can be constructed by the heat input and material properties using Equation 2.3.2:

$$\dot{V}_{heat} = (\varepsilon \cdot P_{Laser} - P_{loss})/(C_p(T_{melt} - T_{Powder}) \cdot \rho) \tag{2.3.2}$$

P_{Laser} is the laser power input; P_{loss} is the heat loss rate from the melt pool; C_p is the specific heat of the material; T_{melt} and T_{Powder} represent the melting temperature and the powder temperature, respectively, before falling into the melt pool; ρ is the density of the material; $\dot{V}_{heat}$ represents the theoretical volume build rate based on the heat input and material choice; and ε is the laser efficiency. LMD parts only consume a portion of the laser power and reflect the rest during the process. Therefore, the laser efficiency varies according to the material reflection rate. Because the two-volume build rate is the same, this relationship can be represented by Equations 2.3.3-2.3.5.

$$\dot{V}_{speed} = \dot{V}_{heat} \tag{2.3.3}$$

$$v \cdot h \cdot D_{Beam} = (\varepsilon \cdot P_{Laser} - P_{loss})/(C_p(T_{melt} - T_{Powder}) \cdot \rho) \quad (2.3.4)$$

$$v = (\varepsilon \cdot P_{Laser} - P_{loss})/(C_p(T_{melt} - T_{Powder}) \cdot \rho) \cdot h \cdot D_{Beam} \quad (2.3.5)$$

The heat caused by fusion is not included in the equation because the melt pool will release the same amount of heat as the part solidifies. The energy management sensor will maintain the heat input to the melt pool, so the table speed value is mostly affected by the layer thickness. From Equation 2.3.5, if the heat terms ($\varepsilon \cdot P_{Laser} - Q_{loss}$) and the material terms ($C_p(T_{melt} - T_{Powder}) \cdot \rho$) remain constant, a higher table speed is required to achieve a lower desired layer thickness. Therefore, if the max table speed is not fast enough, the height control system will not be able to build parts with low layer thicknesses.

3. EXPERIMENT PROCEDURE

3.1 PROPOSED TECHNIQUE

The main idea behind the new technique proposed in this thesis was to use a pyrometer to monitor the current build height of the part during the building process. Figure 3.1 shows the different pyrometer signal levels according to the part current build height. The melt pool has the highest temperature at the top of the part, and the part has a temperature gradient from high to low along the melt pool to the bottom of the part. Therefore, the pyrometer will have the strongest signal when it aims at the melt pool, a lower signal under the melt pool, and almost no signal above the melt pool.

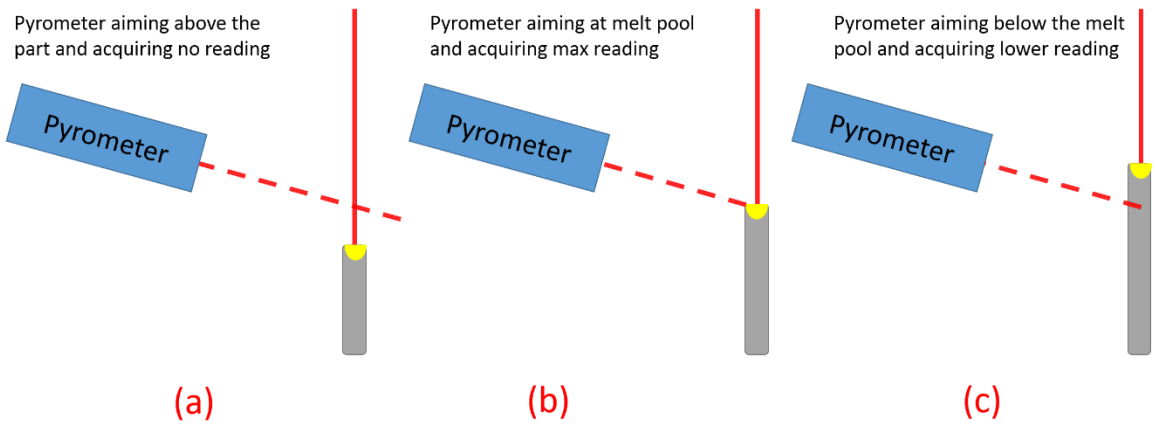

Figure 3.1 Pyrometer signal differs according to part current build height: (a) no signal acquired when aiming above the melt pool; (b) maximum signal acquired when aiming at the melt pool; and (c) low signal when aiming below the melt pool.

Figure 3.2 shows the height control system nomenclature. To apply this idea, the height control system is set up such that the pyrometer axis, powder feed nozzle axis, and laser axis intersects at a location on the substrate. Once the build begins, the Z axes

moves the head assembly up by one layer thickness. In this situation, the pyrometer will lose most of the signal from the melt pool, because it is aim point is now above the melt pool. The height control system will pause the linear table's motion until the pyrometer receives a signal level higher than the set value. The build-up on the part will then be at the desired height. At this moment, the standoff distance is the same as it was at the beginning of the process. The control system would now allow the linear table to continue moving.

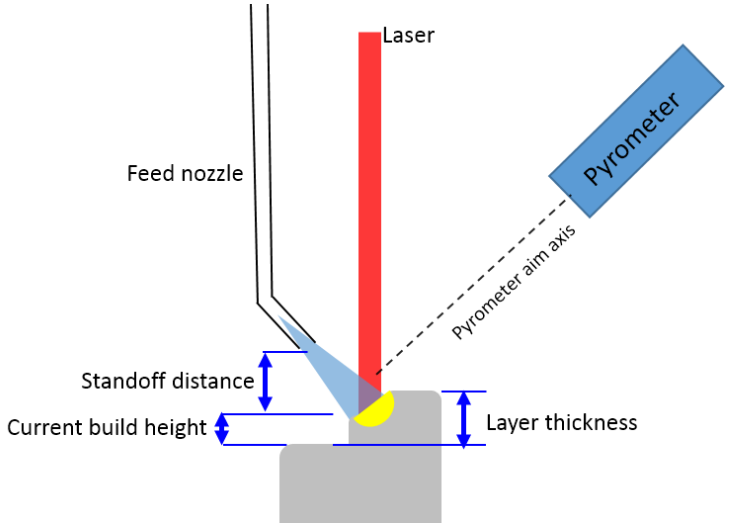

Figure 3.2 Height control system nomenclature. Standoff distance is the distance between feed nozzle and melt pool. Current build height is the part build height on the current layer.

Figure 3.3 is a process flow chart for the proposed technique. During material deposition, when the pyrometer acquires a signal lower than a specific signal level, the LMD system will consider the part too short. The control system will keep the part at its current position until the pyrometer acquires a signal that is higher than the set level. The

designed part is built by repeating this method until reaching the last position of the path of the last layer.

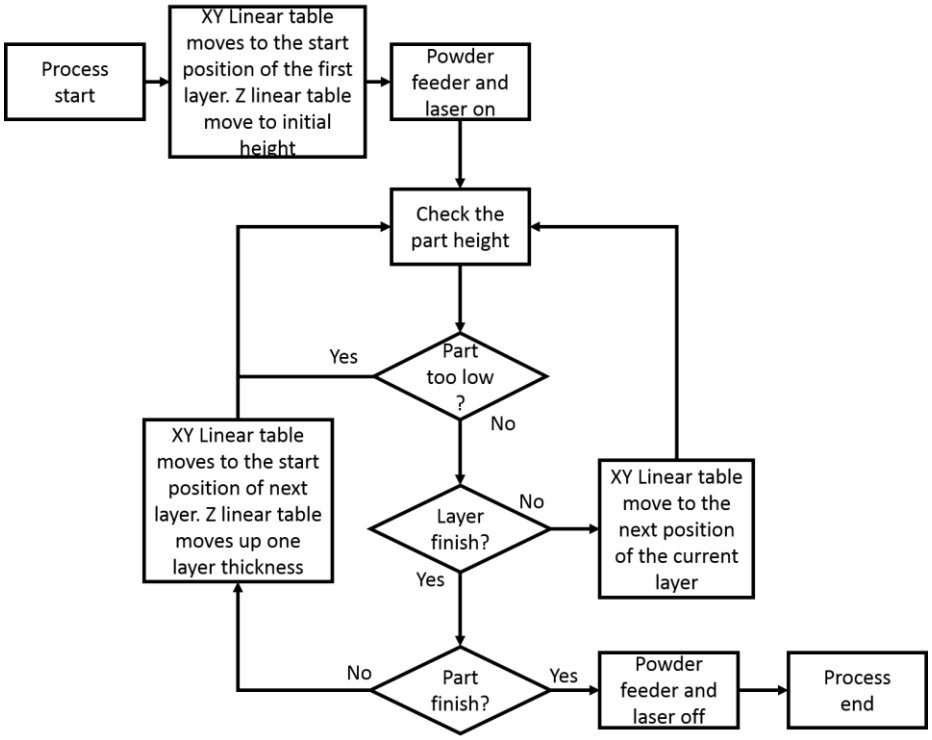

Figure 3.3 LMD process flow chart

3.2 EXPERIMENTAL SETUP

The new LMD system was built using the instruments noted in the following list. All equipment was available in the LAMP lab at the Missouri University of Science & Technology.

- 1kW Yag fiber laser
- 3-axis linear table
- Gaecko stepper driver
- Bay State Technologies Model 1200 Powder Feeder with self-made feeding tube
- Arduino microcontroller board (DUE, UNO, Duemilanove)
- MIKRON MI-GA 5-LO pyrometer

- Energy management sensor

The following parameters were used for the instruments:

- **Laser setpoint**: The energy management sensor used a PID control method to control the laser power level. A higher setpoint of the PID control method means that the system will output higher laser power.
- **Table speed**: The moving speed of linear tables.
- **Layer thickness**: The Z direction increment after finishing each layer of the part during the LMD process.
- **Powder feed rate**: Material feeding speed of the powder feeder.

Figure 3.4 is the system control flow chart.

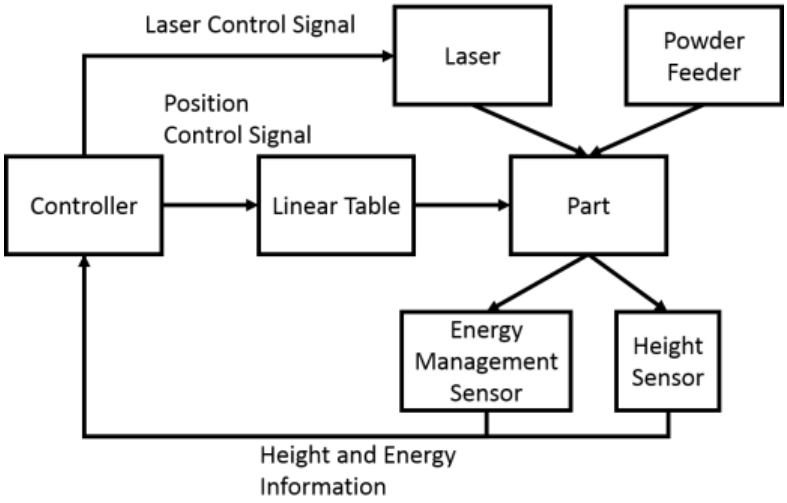

Figure 3.4 System control flow chart

In our experiment, Arduino boards controlled the behaviors of all of the instruments, except for the powder feeder. The feed rate of the powder feeder had to be adjusted and manually turned on and off. Microcontrollers controlled the position of the linear table and the power that the laser was outputting according to the feedback information from the pyrometer and the energy management sensor.

Figure 3.5 is a schematic sketch of sensor deployment. Both sensors had to be aimed at the melt pool.

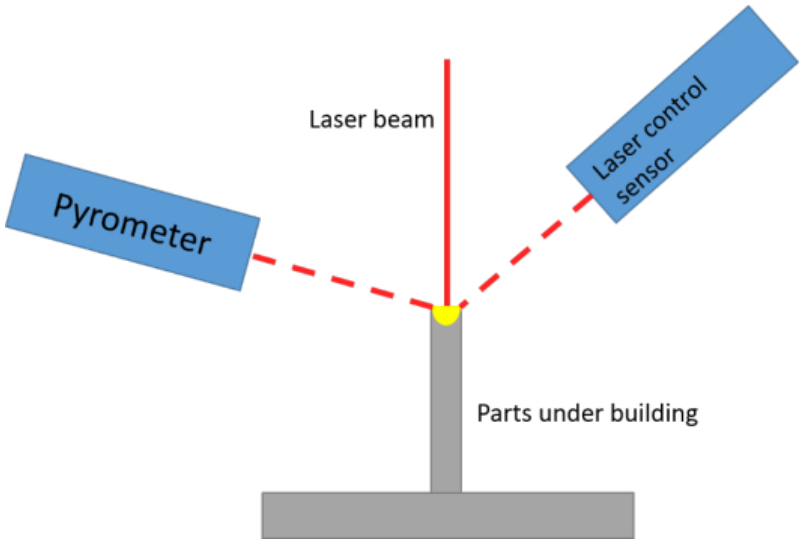

Figure 3.5 Sensor deployment of the height control system. The pyrometer and laser control sensor had to be deployed on different sides of the part to avoid disturbing the receipt of the signal.

3.3 DESIGN OF EXPERIMENT

Two tests were designed to investigate the capability of the height control system on thin wall depositions in terms of accuracy, repeatability, build rate, surface roughness, pore size, and efficiency. The sample parts had thin walls of 20 mm, as shown in Figure 3.6. The test material was 230/325 mesh 316-L stainless steel.

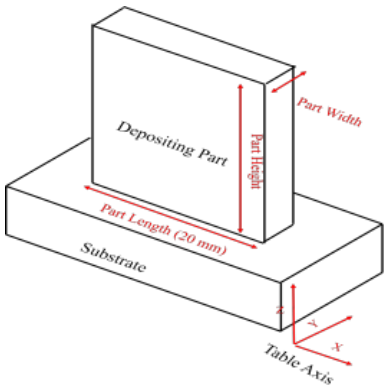

Figure 3.6 Test part dimensions

3.3.1 Accuracy and Repeatability Test. The accuracy and repeatability test measured the consistency and precision of the final part height. This test was conducted under the same system settings except with different set heights. The closer the set height and actual measured height of the parts, the better the accuracy of the height control system. Also, if parts with the same set height have similar actual measured height readings, the system has better repeatability. Table 3.1 lists the test parameter and run order.

Table 3.1 Accuracy and repeatability test table.

Run #	Part height	Table set speed	Layer thickness	Power setpoint	Powder flow rate
	mm	mm/s	mm	No unit	g/min
1	10	15	0.2	175	6.82
2					
3					
4	15				
5					
6					
7	20				
8					
9					

3.3.2 Center Composite Test. One goal of the height control system was to control the build efficiency, build rate, and surface quality of the LMD system. The performance of the system was affected primarily by the table speed, powder flow rate, laser power, and layer thickness. Because the control system controlled the table speed, only three input variables remained, which were the powder flow rate, laser power, and layer thickness. This experiment was designed in a central composite test fashion with three factors and five level. Such a design can reduce the number of test runs and facilitate measurements of the efficiency, build rate, pore size, and surface quality under different conditions. Table 3.2 shows the test details.

Table 3.2 Central composite test table.

Test #	Run #	Part height mm	Table set speed mm/s	Power set point No unit	Layer thickness mm	Powder flow rate g/min
1	16	10	15	175	0.2	6.82
2	11			175	0.2	6.82
3	15			175	0.2	6.82
4	13			175	0.34	6.82
5	9			175	0.06	6.82
6	12			175	0.2	9.32
7	17			175	0.2	4.85
8	8			225	0.3	8.53
9	7			225	0.3	5.03
10	3			225	0.1	8.53
11	4			225	0.1	5.03
12	5			125	0.3	8.53
13	2			125	0.3	5.03
14	6			125	0.1	8.53
15	1			125	0.1	5.03
16	10			246	0.2	6.82
17	14			104	0.2	6.82

3.4 MEASURING PROCEDURE

3.4.1 Length, Width, and Height. Figure 3.7 shows the measuring position of the length, width, and height of the part. A caliper served as the measuring tool. The height was measured from the top of the part to the substrate at the center of the part. The length was measured along the x axis in the middle of the part height-wise. The width was measured along the y axis at the middle of part length-wise.

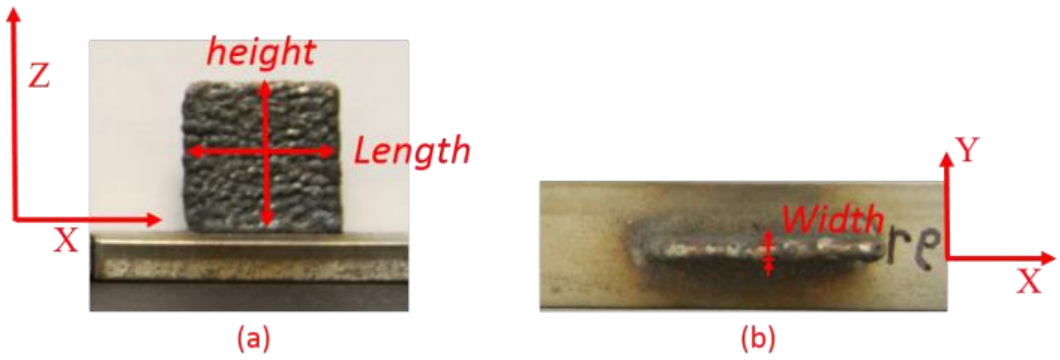

Figure 3.7 Example of part length, width, and height measurement: (a) Front view of the part showing the positions of height and length measurements; (b) Top view of the part showing the position of the width measurement.

3.4.2 Height Build Rate, Volume Build Rate, and Material Efficiency. The height build rate estimates how fast the process can build the part along the Z axis. The volume build rate estimates how fast the process can build the full volume of the part. Material efficiency is the ratio of the actual part mass to the total powder mass used in the entire process.

The height build rate, volume build rate, and material efficiency of parts was estimated using the following factors: part height (H), part length (L), part width (W), material density ($\boldsymbol{\rho}$), powder flow rate (M), and process time (T). Equations 3.4.2.1-

3.4.2.3 were used to estimate the height build rate, volume build rate, and material efficiency. The density of the 316-L stainless steel was 8g/cc.

$$Height\ build\ rate: \dot{H} = {}^{H}/_{T} \quad (3.4.2.1)$$

$$Volume\ build\ rate: \dot{V} = {}^{H \cdot L \cdot W}/_{T} \quad (3.4.2.2)$$

$$Material\ efficiency: E = {}^{H \cdot L \cdot W \cdot \rho}/_{M \cdot T} \quad (3.4.2.3)$$

3.4.3 Surface Roughness. Surface point clouds were acquired by a NEXTENGINE 3D scanner, which was not designed to measure surface roughness. It will give inaccurate results for parts with very fine surface finishes. However, the LMD parts made using the height control system had much higher surface roughness than fine machine parts. Therefore, this scanner was able to measure their surface roughness. The Ra value was used to determine the surface roughness. As Figure 3.8 illustrates, the Ra value is the arithmetic average of the normal distance between surface points to the best fit plane. Ra was calculated using Equation 3.4.3.1, where $\boldsymbol{y_i}$ is the distance between surface points i and the fitted plane, and n is the total number of surface points.

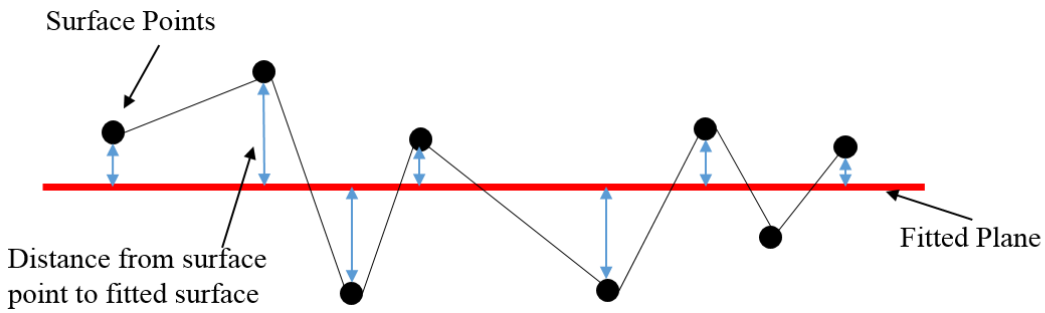

Figure 3.8 Schematic diagram of surface roughness: Ra value is the arithmetic average of the normal distance between surface points to the best fit plane.

$$R_a = \frac{1}{n}\sum_{i=1}^{n}|y_i| \qquad (3.4.3.1)$$

Figure 3.9 shows an example of a surface point cloud and its fitted plane. The red dots represent the surface point cloud, and the blue plane is the plane fitted according to the point cloud. The final surface roughness value was the average of the RA on both sides of the part's thin wall.

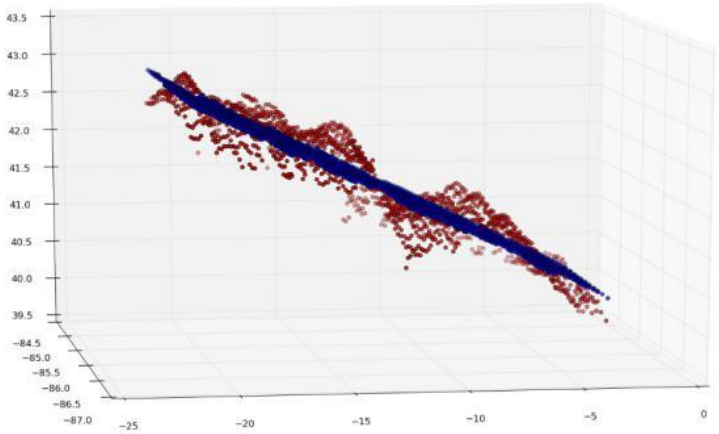

Figure 3.9 Example of a surface point cloud and its fitted plane. Red dots represent the part's surface point cloud, and the blue plane is the fitted plane.

3.4.4 Pore Size. The part's pore size was estimated using an optic microscope. First, the part was cut, polished, and etched. It was cut in half in the same direction as the part height measuring direction shown in Figure 3.10.

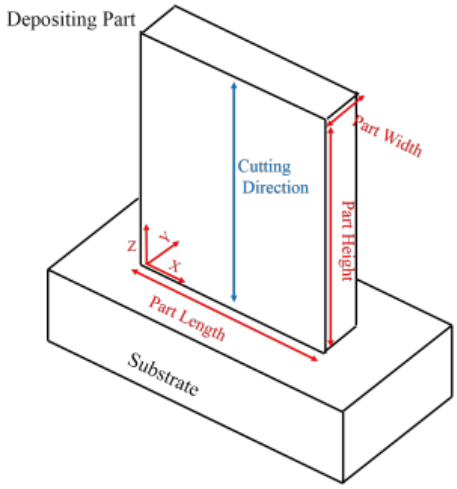

Figure 3.10 Example of part cutting direction for porosity examination preparation: Blue line shown in the middle of the X-Z plane is the cut direction.

Etchant chemicals were 0.75 g molybdic acid, 25ml hydrochloric acid, 25ml nitric acid, and 25ml de-ionized water. The pore size was examined on this cross section. The polishing process may remove whole part materials if the X-Z plane surface is used to examine the porosity, so the three images were taken from the top, center, and bottom of each part, respectively. Image J was used to measure the pore size on the images.

4. RESULTS AND DISCUSSION

4.1 ACCURACY AND REPEATABILITY TEST RESULTS

The experiments described in Chapter 3 were conducted, and the results are discussed here. Figure 4.1 shows the parts made using the height control system. The part heights from left to right were 20mm, 15mm, and 10mm. Table 4.1 lists additional data.

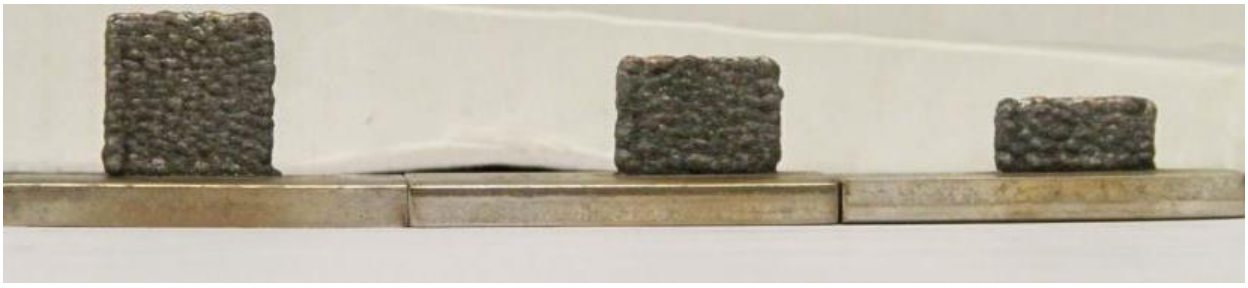

Figure 4.1 Parts made using the height control system. The part heights from left to right are 20mm, 15mm, 10mm.

Table 4.1 Accuracy and repeatability test results

Accuracy and Repeatability Test							
Run #	Part height	Measured height	Measured length	Measured width	Build time	Difference from the set height	Roughness
	mm	mm	mm	mm	sec	mm	Ra(Microns)
1	10	9.9	22.05	1.94	391.81	-0.1	93.05
2	10	9.88	21.85	1.96	392.95	-0.12	106.35
3	10	10.1	21.78	1.9	401.82	0.1	116.85
4	15	14.51	21.78	1.92	593.42	-0.49	98.9
5	15	14.92	21.25	1.96	610.03	-0.08	99.55
6	15	15.45	21.79	2.05	644.01	0.45	99.15
7	20	21.02	22.02	1.93	821.93	1.02	100.2
8	20	20.93	21.84	1.99	916.94	0.93	98.85
9	20	20.79	21.72	1.87	922.44	0.79	97

All parts had similar lengths and widths. Length differences were within 0.53 mm, and width differences were within 0.18 mm. The height differences were 0.22 mm in 10 mm parts, 0.94 mm in 15 mm parts, and 0.23 mm in 20 mm parts. The differences between the set height and the actual height were +- 0.12mm in 10 mm parts, +- 0.49 in 15mm parts, and +- 1.02 mm in 20 mm parts. The accuracy of the part could be improved by better securing the part substrate in same position. Figure 4.2 shows a part made under the same parameters as in the tests previously described, but without the control system.

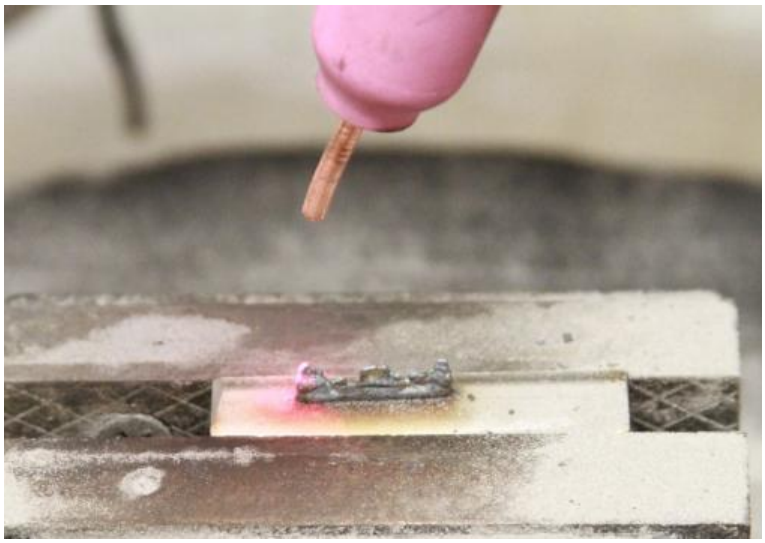

Figure 4.2 Parts made without height control system. The standoff distance increased quickly after a few layers. The part stopped being built up after the powder stream completely missed the melt pool.

As Figure 4.2 illustrates, this part was not built higher after a certain layer because the layer thickness and table speed were set too high. This proves that the height control system can correct for incorrect parameters that may have been picked for the process. This kind of correction cannot ensure that the part will be made in the most efficient way, but it helps when making parts using unfamiliar materials with unknown properties.

4.2 CENTRAL COMPOSITE TEST RESULT

As noted in the discussion of the experimental design, efficiency tests also were performed. Table 4.2 shows the results of these tests.

Table 4.2 Central composite test results

Central Composite Test Results							
Test #	Powder set point	Layer thickness	Powder flow rate	Measured height	Measured length	Measured width	Building time
		mm	g/min	mm	mm	mm	Sec.
1	175	0.2	6.82	9.7	21.8	1.94	391.36
2	175	0.2	6.82	9.5	21.4	1.9	438.65
3	175	0.2	6.82	9.7	22.02	2.05	389.59
4	175	0.34	6.82	9.89	21.8	2.23	418.54
5	175	0.06	6.82	10.07	21.09	0.86	301.101
6	175	0.2	9.32	9.9	21.59	1.85	311.01
7	175	0.2	4.85	9.63	20.42	1.77	651.46
8	225	0.3	8.53	9.57	21.83	2.33	344.62
9	225	0.3	5.03	9.52	21.3	2.39	653.33
10	225	0.1	8.53	10.32	21.59	1.47	300.46
11	225	0.1	5.03	9.58	21.5	1.8	685.57
12	125	0.3	8.53	10.11	21.52	1.69	318.92
13	125	0.3	5.03	9.8	20.47	1.42	576.71
14	125	0.1	8.53	9.9	20.51	0.99	248.91
15	125	0.1	5.03	9.44	20.67	1.1	401.29
16	246	0.2	6.82	9.43	22.3	2.22	463.27
17	104	0.2	6.82	9.75	21.03	1.14	322.06

Table 4.2 Central composite test results(cont.)

Central Composite Test Result (cont.)								
Test #	Powder set point	Layer thickness	Powder flow rate	Volume (approximate)	Volume build rate	Height build rate	Efficiency of material	Roughness
		mm	g/min	mm^3	mm^3/s	um/s	(%)	RA(Microns)
1	175	0.2	6.82	410.23	1.05	24.79	7.38%	97.5
2	175	0.2	6.82	386.27	0.88	21.66	6.20%	101.4
3	175	0.2	6.82	437.87	1.12	24.90	7.91%	92.4
4	175	0.34	6.82	480.79	1.15	23.63	8.08%	126.2
5	175	0.06	6.82	182.64	0.61	33.44	4.27%	72.9
6	175	0.2	9.32	395.42	1.27	31.83	6.55%	96.5
7	175	0.2	4.85	348.06	0.53	14.78	5.29%	106.55
8	225	0.3	8.53	486.77	1.41	27.77	7.95%	136.9
9	225	0.3	5.03	484.63	0.74	14.57	7.08%	132.1
10	225	0.1	8.53	327.53	1.09	34.35	6.13%	96.5
11	225	0.1	5.03	370.75	0.54	13.97	5.16%	118.75
12	125	0.3	8.53	367.69	1.15	31.70	6.49%	85
13	125	0.3	5.03	284.86	0.49	16.99	4.71%	76.95
14	125	0.1	8.53	201.02	0.81	39.77	4.54%	74.05
15	125	0.1	5.03	214.64	0.53	23.52	5.10%	68.05
16	246	0.2	6.82	466.84	1.01	20.36	7.09%	137.2
17	104	0.2	6.82	233.75	0.73	30.27	5.11%	60.4

Figures 4.3-4.5 indicate that the part width was effected mainly by the laser power and layer thickness setting. A higher heat input potentially can create a larger melt pool, and a higher layer thickness setting will cause the laser to heat at the same position longer. Therefore, both the higher laser setpoint and layer thickness setting led to wider parts.

Theoretically, the melt pool cools faster when more powder is fed into it. However, the power management sensor increased the laser power when the parts cooled too fast. Therefore, the powder feed rate did not have a significant effect on the part width in the current test range.

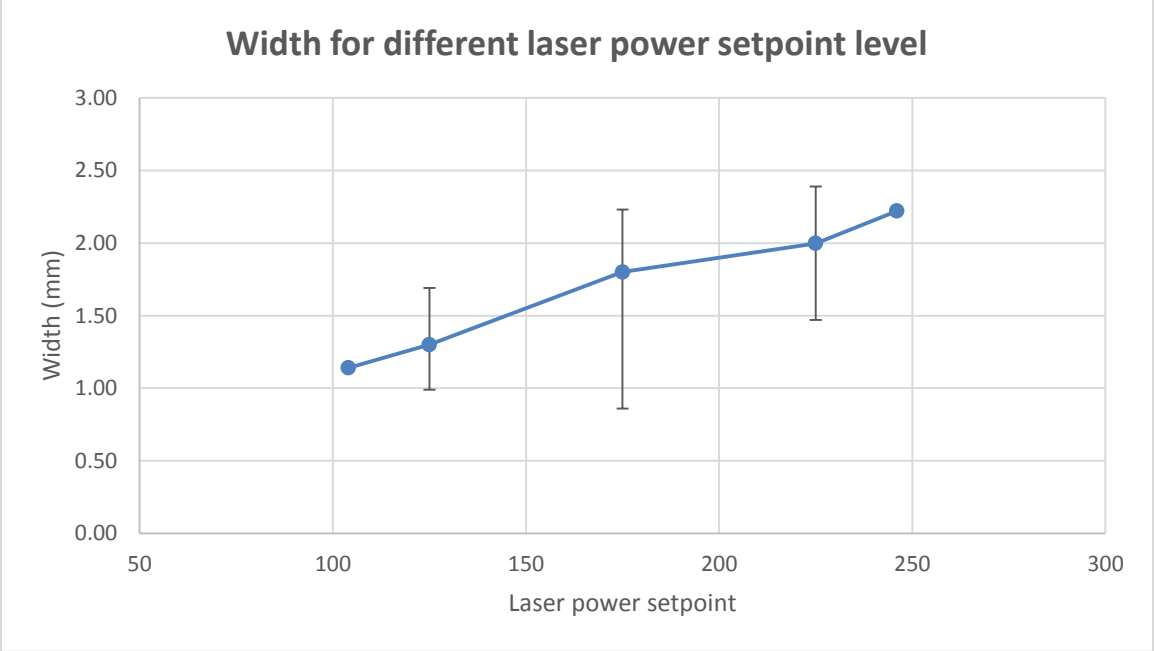

Figure 4.3 Width for different laser power setpoint levels

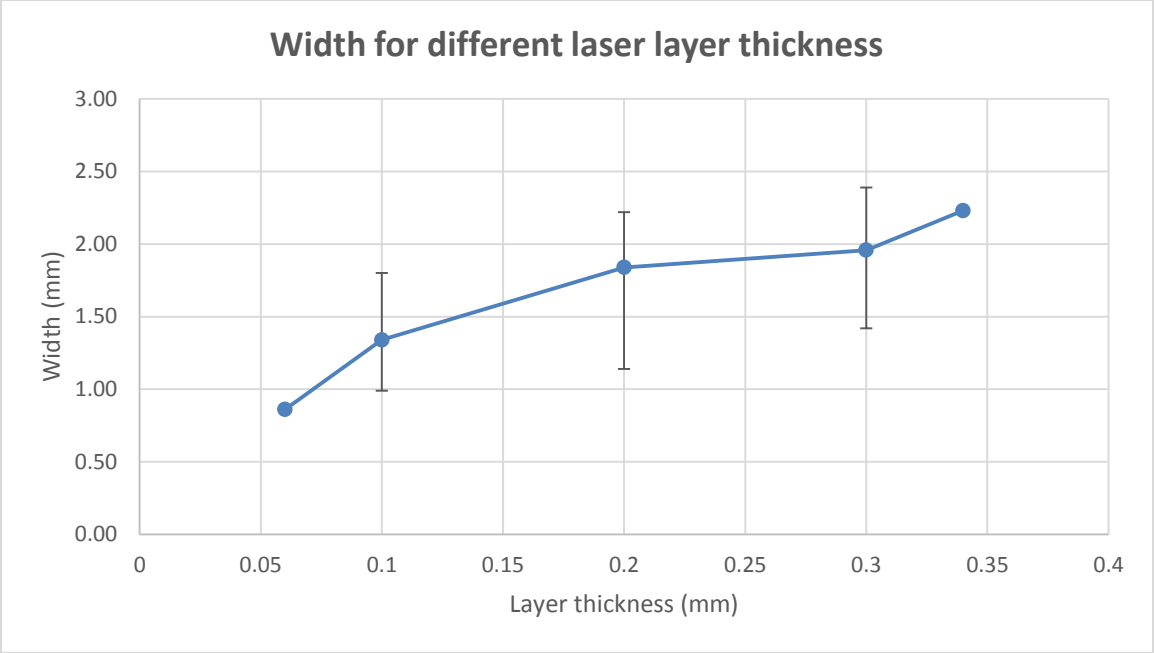

Figure 4.4 Width for different laser layer thicknesses

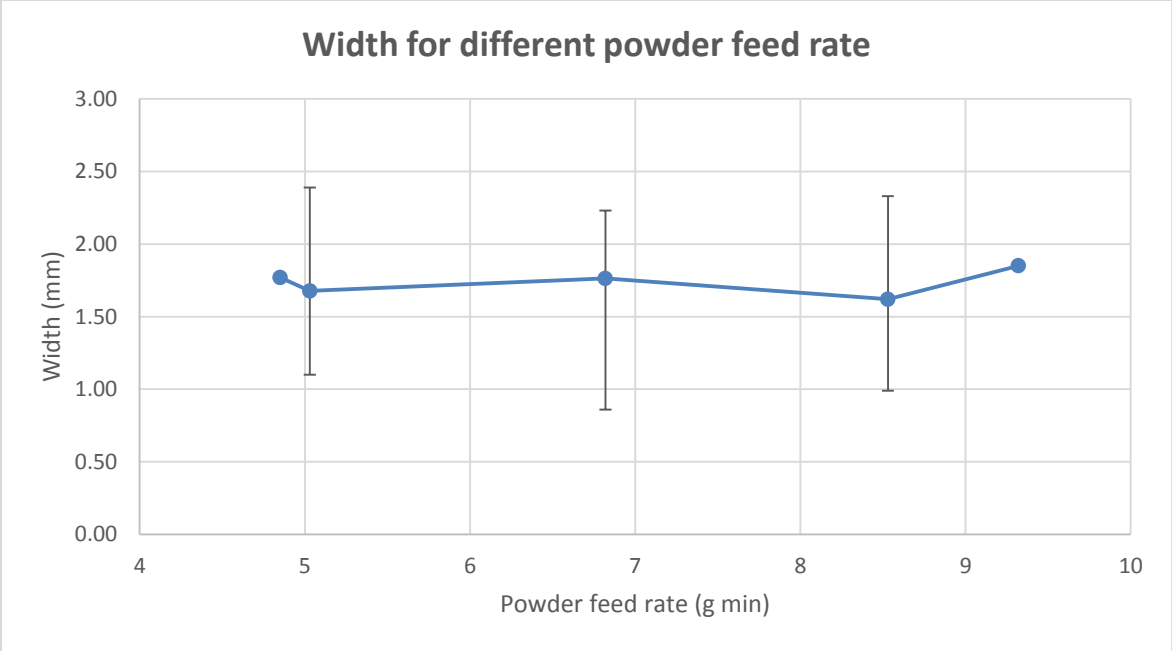

Figure 4.5 Width for different powder feed rates

Figures 4.6-4.8 show that the part height build rate differed under different settings. The height build rate was higher when the laser power setpoint and the layer thickness were lower, and the powder feed rate was higher. The lower laser power setpoint caused lower laser power output. The laser aimed at the same position for a shorter amount of time when the height control system had a lower layer thickness setting. Therefore, the lower laser power and the lower layer thickness caused the smaller melt pool, lower melt pool size, and higher part cooling rate. The melting material liquid had higher viscosity when the melt pool temperature was lower. The melting material with the higher viscosity and cooling rate tended to solidify where the laser melted it. Therefore, the LMD part tended to be built more height-wise than width-wise when the LMD system had a lower power setpoint and layer thickness.

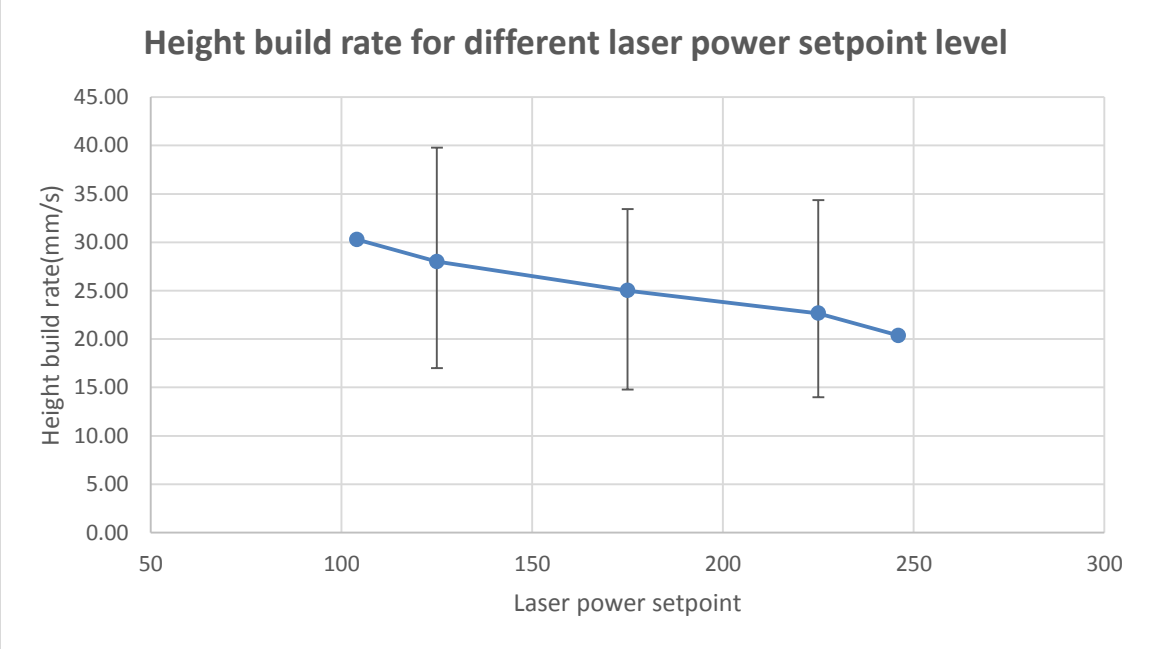

Figure 4.6 Height build rate for different laser power setpoint levels

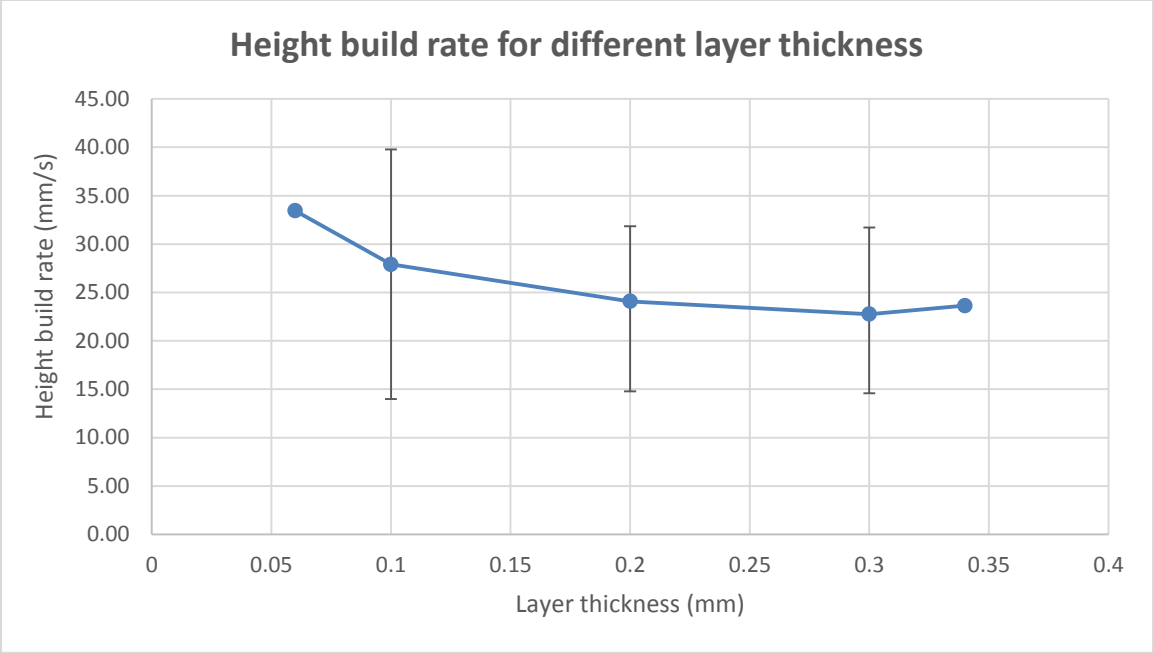

Figure 4.7 Height build rate for different layer thicknesses

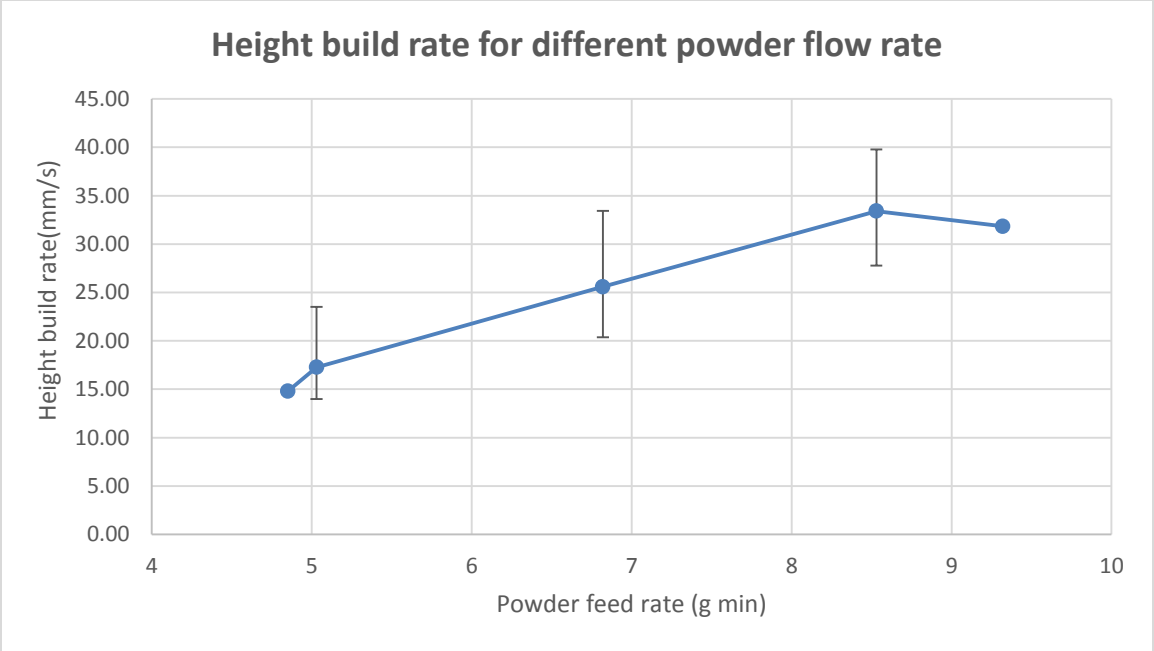

Figure 4.8 Height build rate for different powder feed rates

As indicated in Figures 4.9-4.11, the volume build rate increased with a higher power setpoint, layer thickness, and powder flow rate. The high laser power setpoint and layer thickness caused a larger melt pool and wider parts. The melt pool powder capturing rate increased when the melt pool was larger. The volume build rate increased when both the melt pool powder capturing rate and the powder feed rate increased.

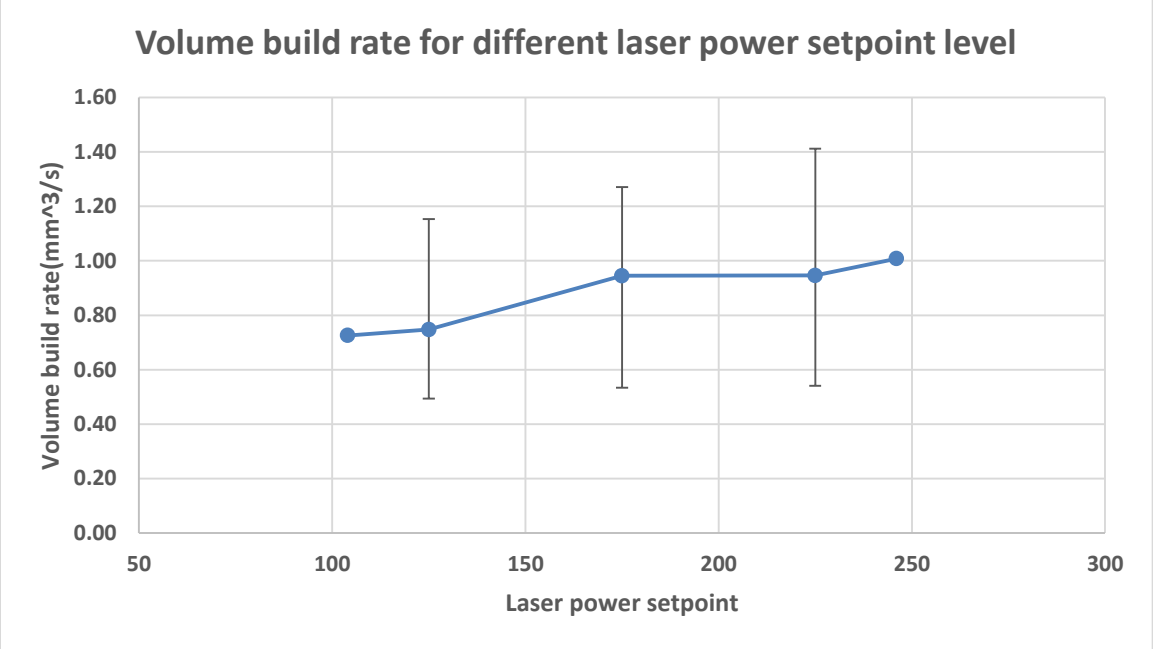

Figure 4.9 Volume build rate for different laser power setpoint levels

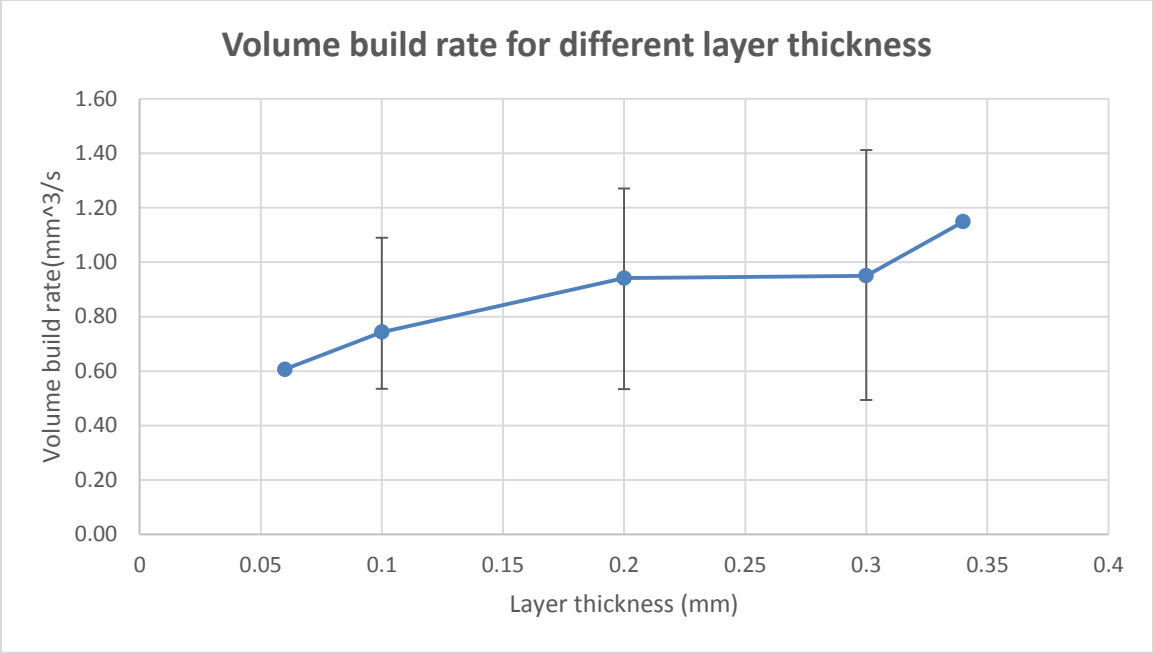

Figure 4.10 Volume build rate for different layer thicknesses

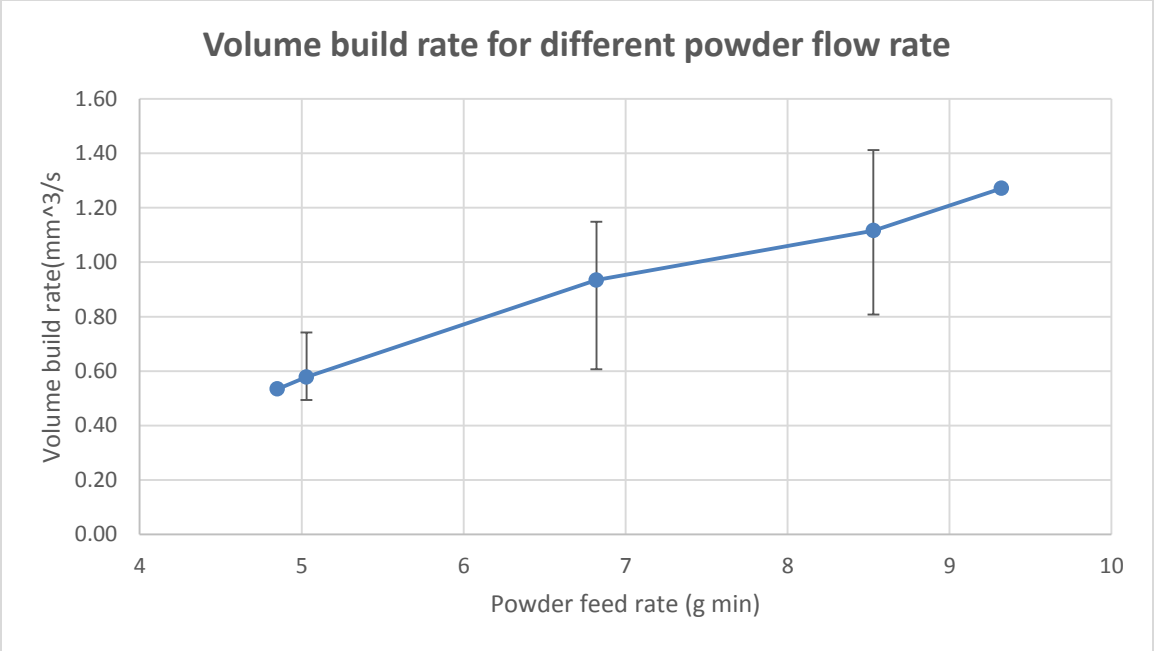

Figure 4.11 Volume build rate for different powder feed rates

Figures 4.12-4.14 show that lower laser power, layer thickness, and powder feed rates yielded a finer surface roughness. Lower power and layer thickness caused less heat input to the same position, and a higher powder feed rate cooled the part faster. Therefore, the LMD process created smaller melting beads. The LMD process with height control system deposited more melting beads to build a part layer when the melting beads were smaller. The parts made in this way had finer surfaces, as illustrated in Figure 4.15.

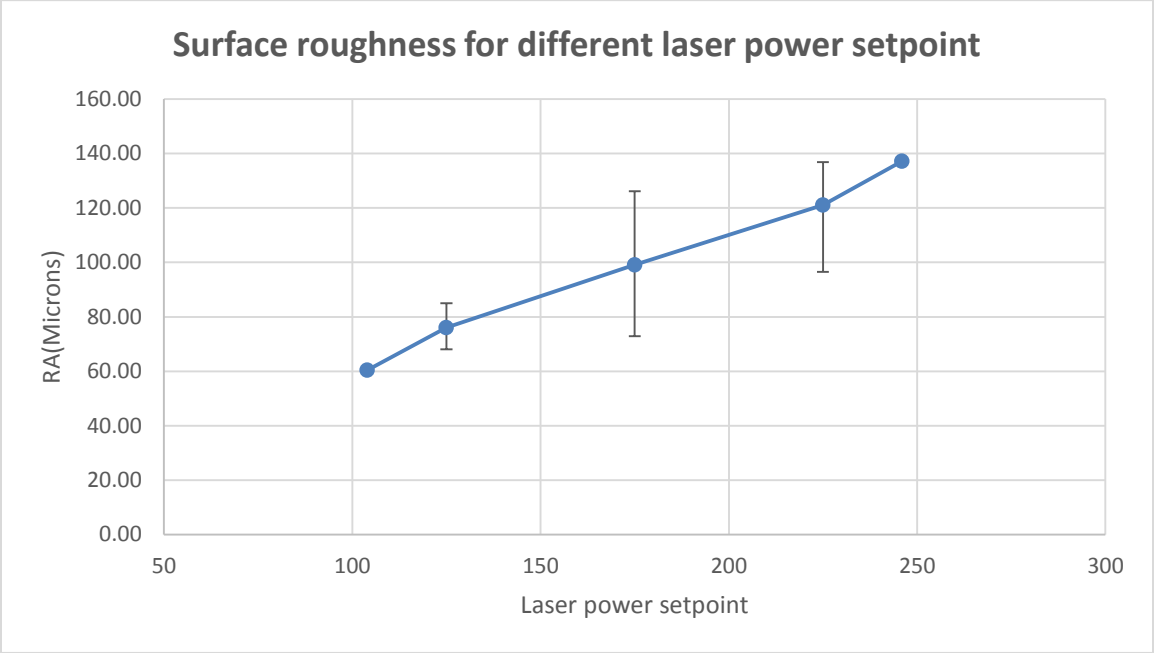

Figure 4.12 Surface roughness for different laser power setpoints

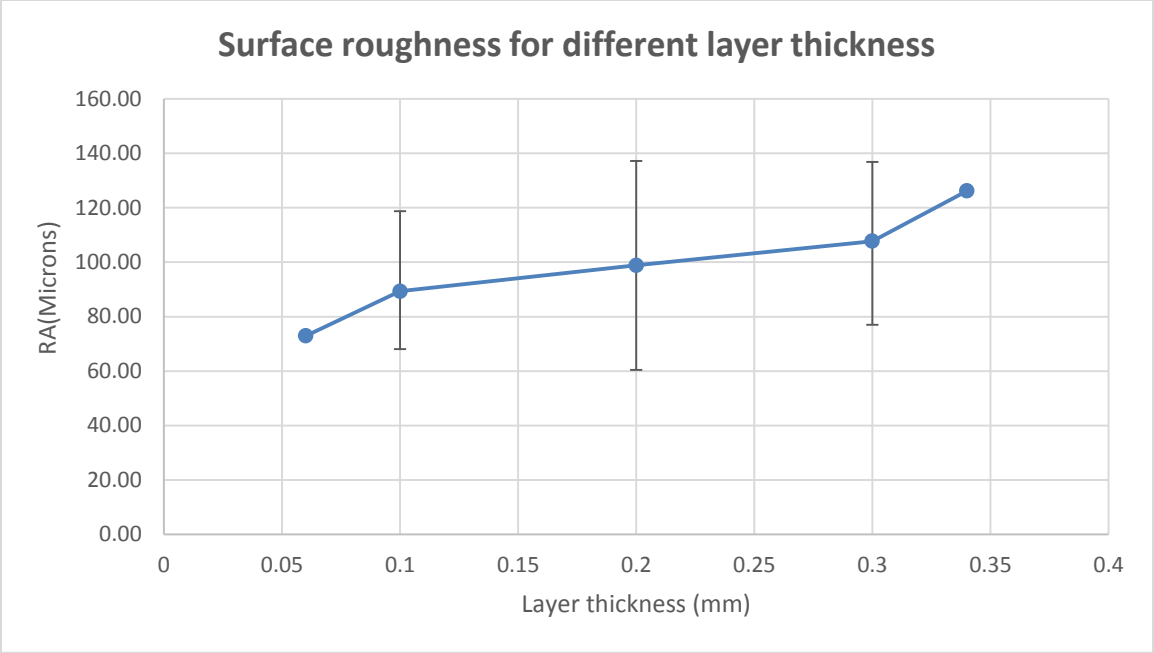

Figure 4.13 Surface roughness for different layer thicknesses

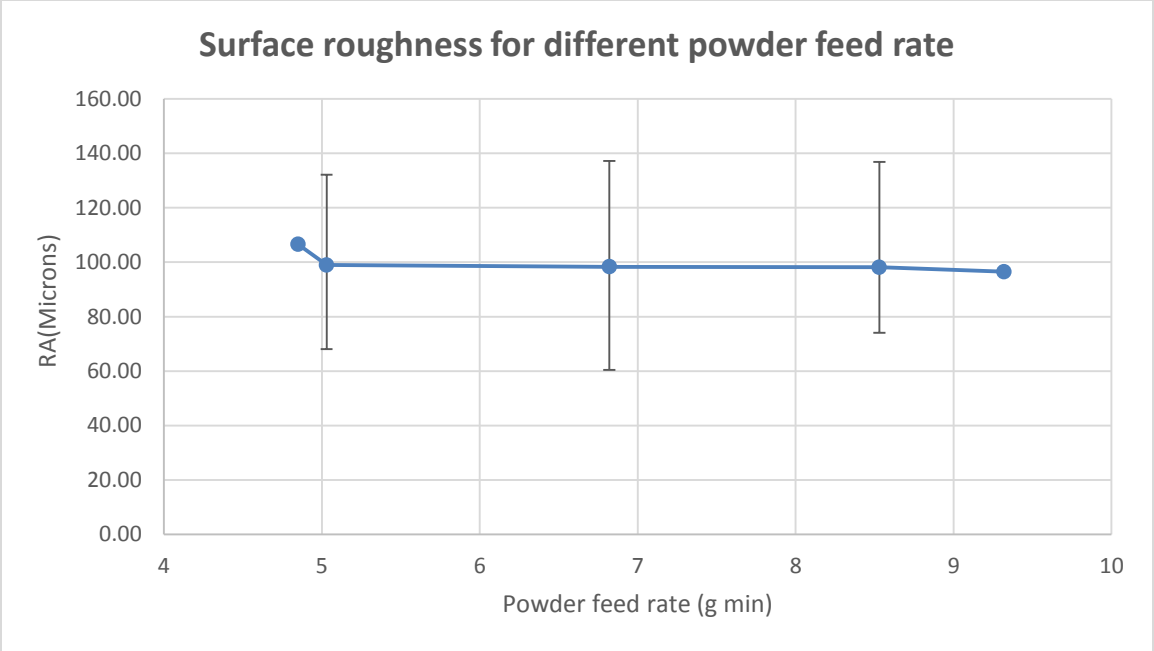

Figure 4.14 Surface roughness for different powder feed rates

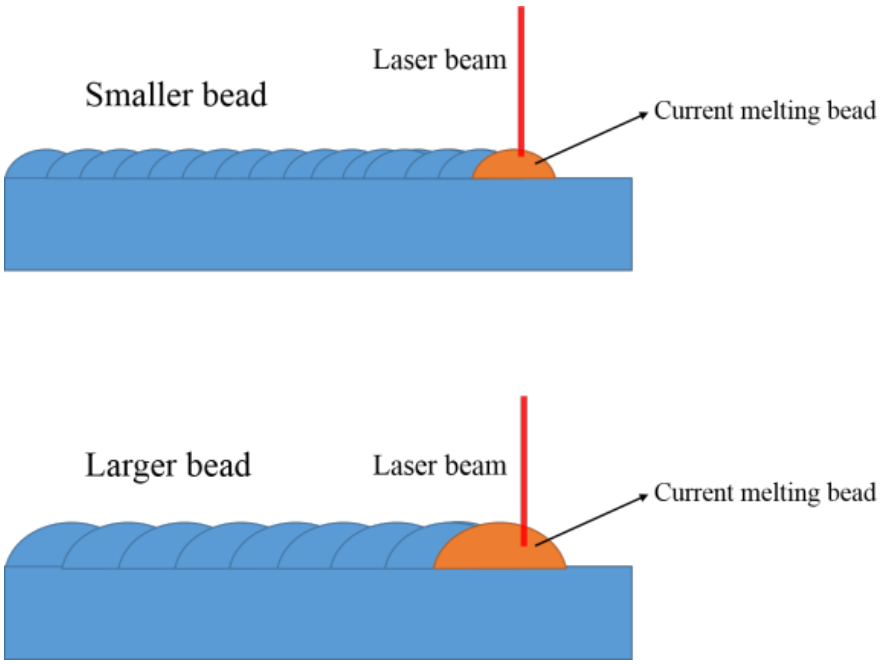

Figure 4.15 Part surface roughness with different melting bead sizes. Parts made with smaller beads have finer surfaces.

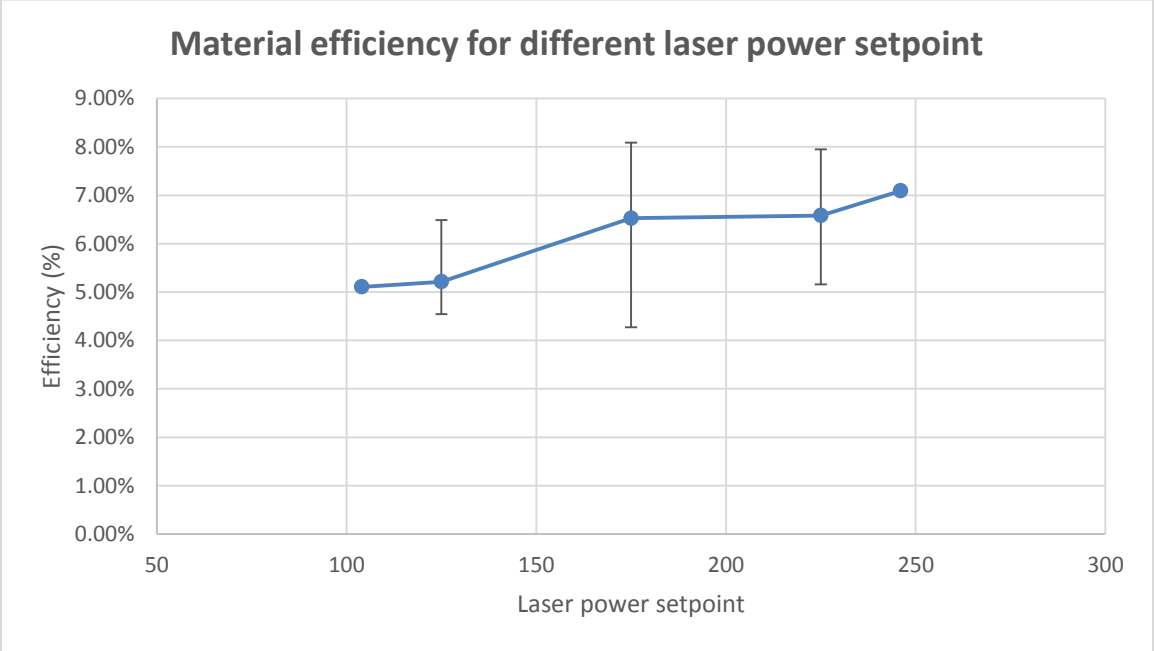

Figure 4.16 Material efficiency for different laser power setpoints

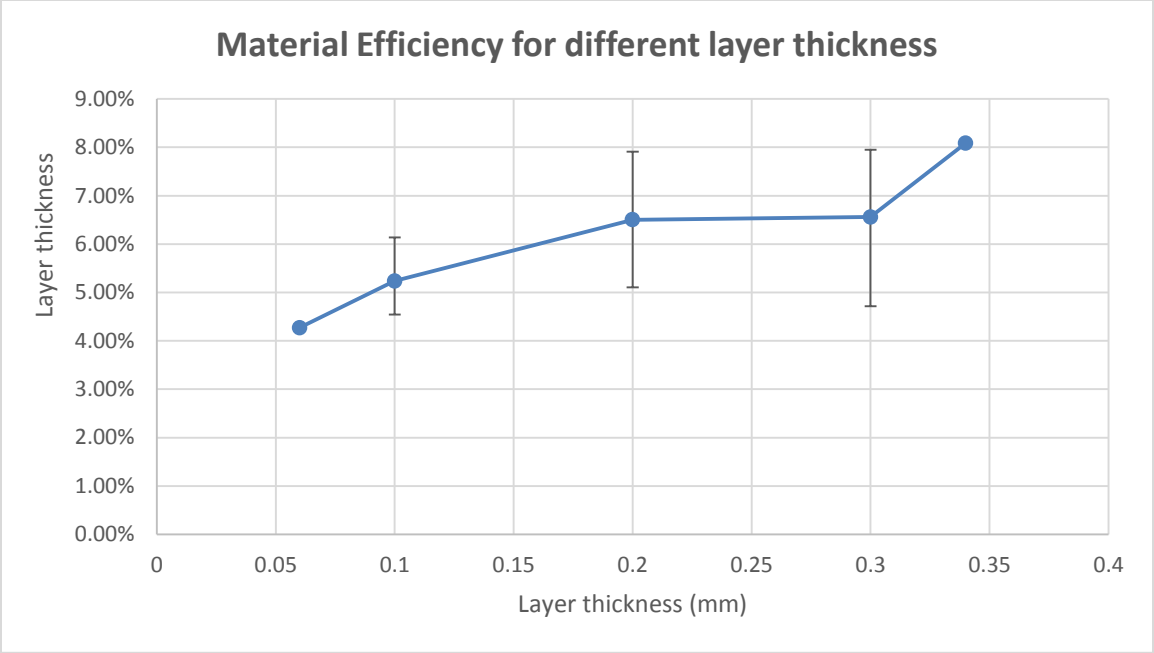

Figure 4.17 Material efficiency for different layer thicknesses

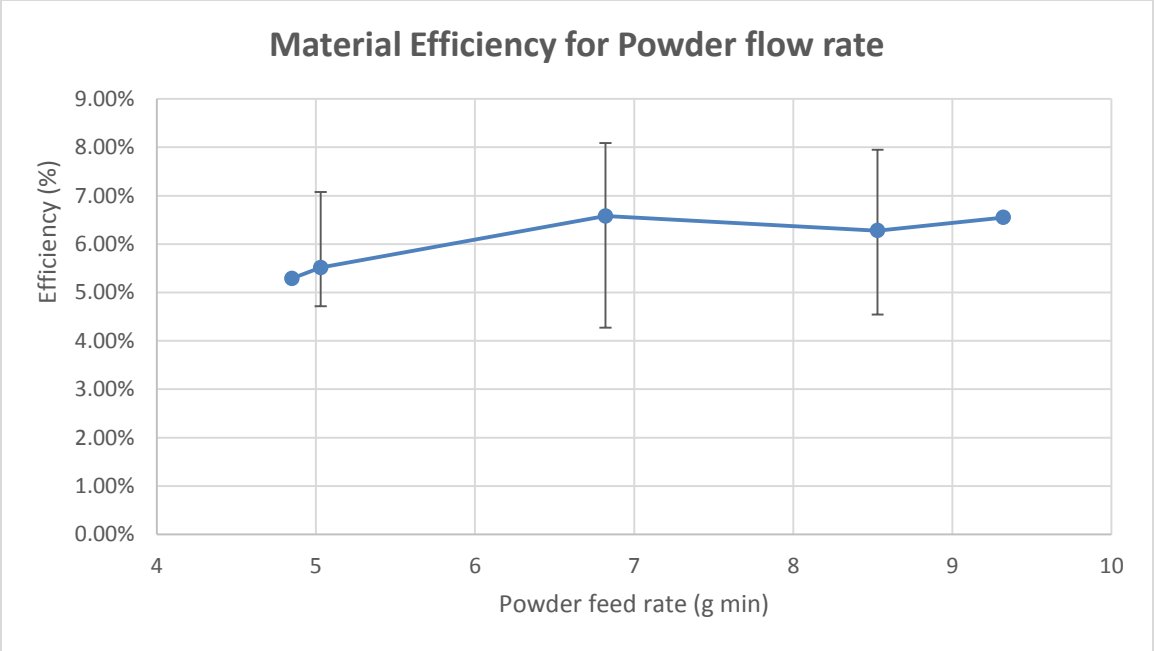

Figure 4.18 Material efficiency for powder flow rates

A hypothesis test for the factor significance was conducted under python with the numPy library. Table 4.3 lists the test results.

Table 4.3 Hypothesis test for efficiency difference

Factor	Regression Coefficient	Std. Error	t Value	Pr(>|t|)
Power	-4.680e-05	4.177e-05	-1.120	0.2828
Powder	2.457e-03	9.370e-04	2.622	0.0211
Layer thickness	2.568e-02	3.770e-03	6.812	1.24e-05

The results indicate that power was less significant in altering the efficiency of material deposition. The powder feed rate and layer thickness, however, affected the efficiency significantly. Power is controlled by the energy management sensor, which will try to lower the power output of the laser when the layer thickness is high. Therefore, the test range may not have been large enough to show the effect of the power setpoint. Both the powder feed rate and the layer height had an estimate regression coefficient, meaning that larger power and feed rate settings would increase the material efficiency in the current range. However, this situation will not always be true because the powder stream exiting the powder feed tube will eventually completely miss the melt pool when the layer thickness is too high. Because a higher layer thickness causes a higher part thickness and larger melting area, the powder has a better chance of landing on the melting area. A higher powder feed rate causes the part to be built faster and better maintains the standoff distance at an optimal range, therefore improving efficiency.

4.3 PORE SIZE

The pore sizes of two thin parts, two thick parts in the central composite test, and one uncontrolled part were examined. Figures 4.19-4.23 depict cross-sections of the parts after polishing and etching. Only pores with a diameter larger than 0.002 mm were detected. The results in Table 4.4 show that the pores found in the height controlled parts were larger than in the uncontrolled part. The inconsistency of the table speed may have been the major reason for these pore size differences. The height control system adjusted the table speed according to the pyrometer reading. The inconsistency of the table movement caused the melting pool to cool at different speeds during the LMD process. Porosity mainly occurred when the part cooled too fast. The gas inside the part could not escape before the melting material solidified. When the linear table of the LMD system moved too fast over some period of time during the process, the chance for larger pores to develop inside the part increased.

The laser output heat into the same position for a shorter amount of time and cooled faster when building thicker parts than when building thinner parts. Theoretically, thinner parts are more likely to have higher porosity and larger pores than thicker parts. However, the maximum pore size was not significantly different between the thinner parts and the thicker parts according to the results in Table 4.4. This may suggest that the pore size is affected mainly by the inconsistent table movement in the current test range.

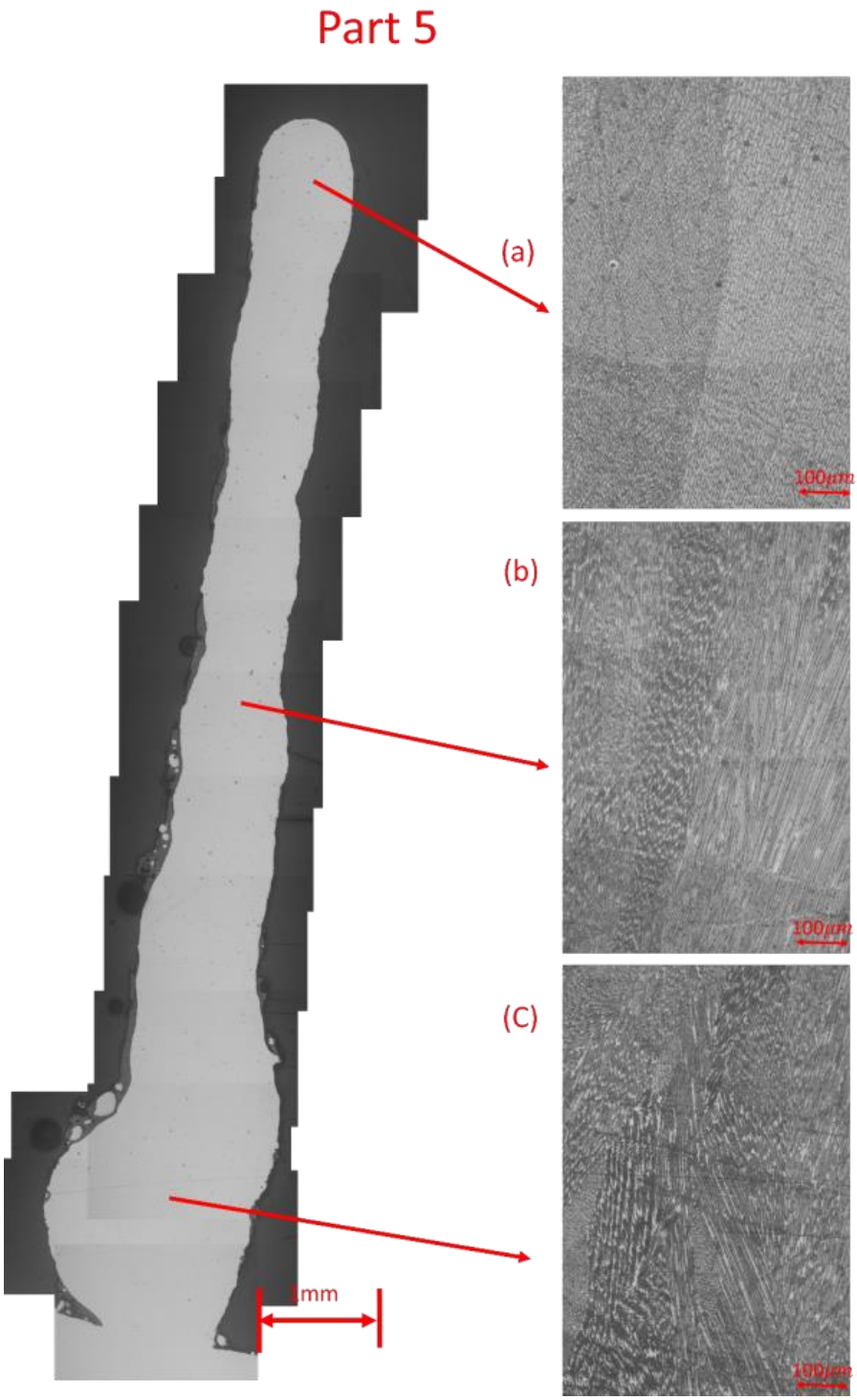

Figure 4.19 Microscopic images of sample 5: The figure on the left is the microscopic image before etching. The gray region is the sample. Images a-c are images after etching. Image (a) was taken from the top of the sample, image (b) from the center of the sample, and image (b) from the bottom of the sample.

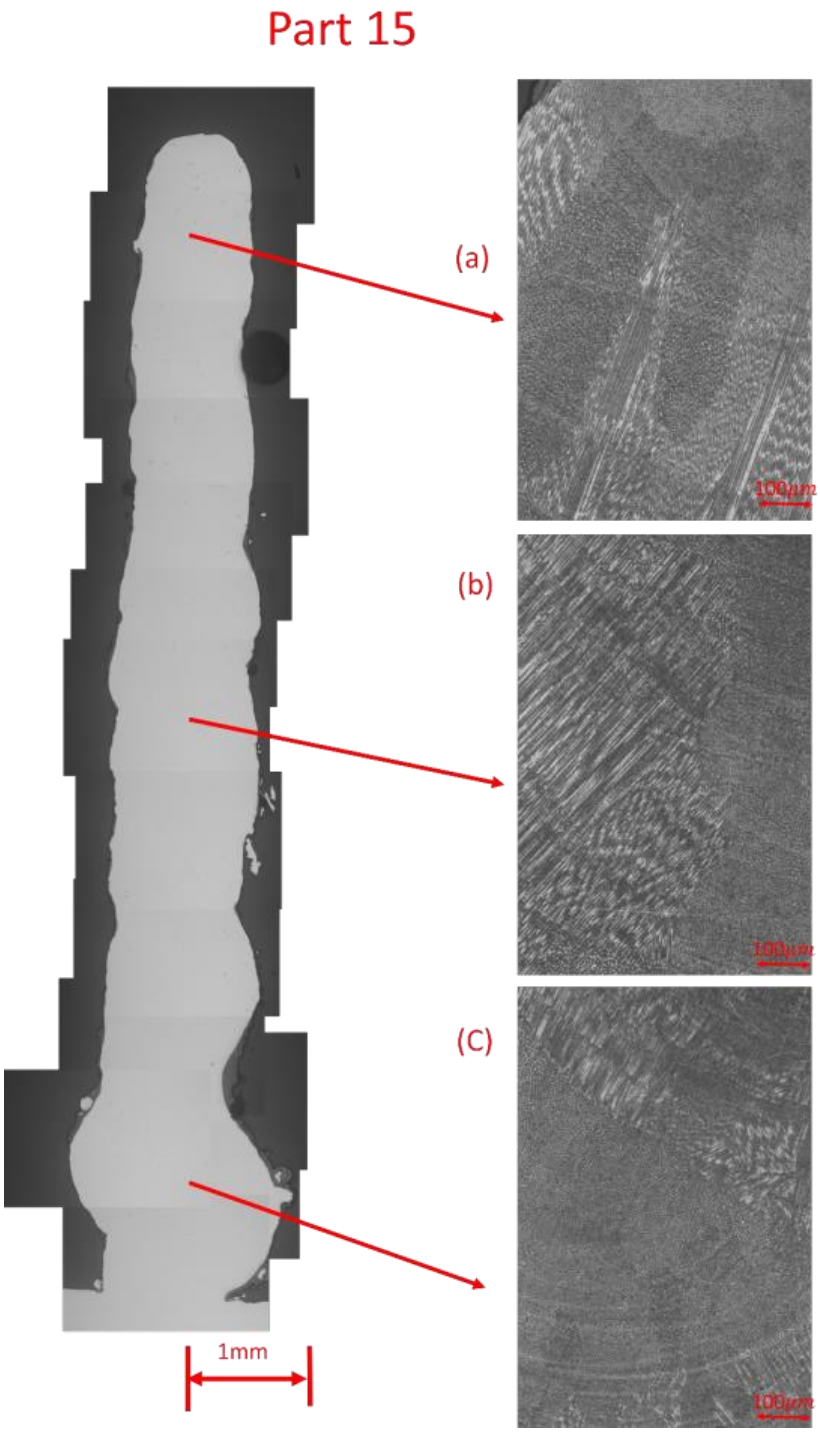

Figure 4.20 Microscopic images of sample 15. The figure on the left is the microscopic image before etching. The gray region is the sample. Images a-c are images after etching. Image (a) was taken from the top of the sample, image (b) from the center of the sample, and image (b) from the bottom of the sample.

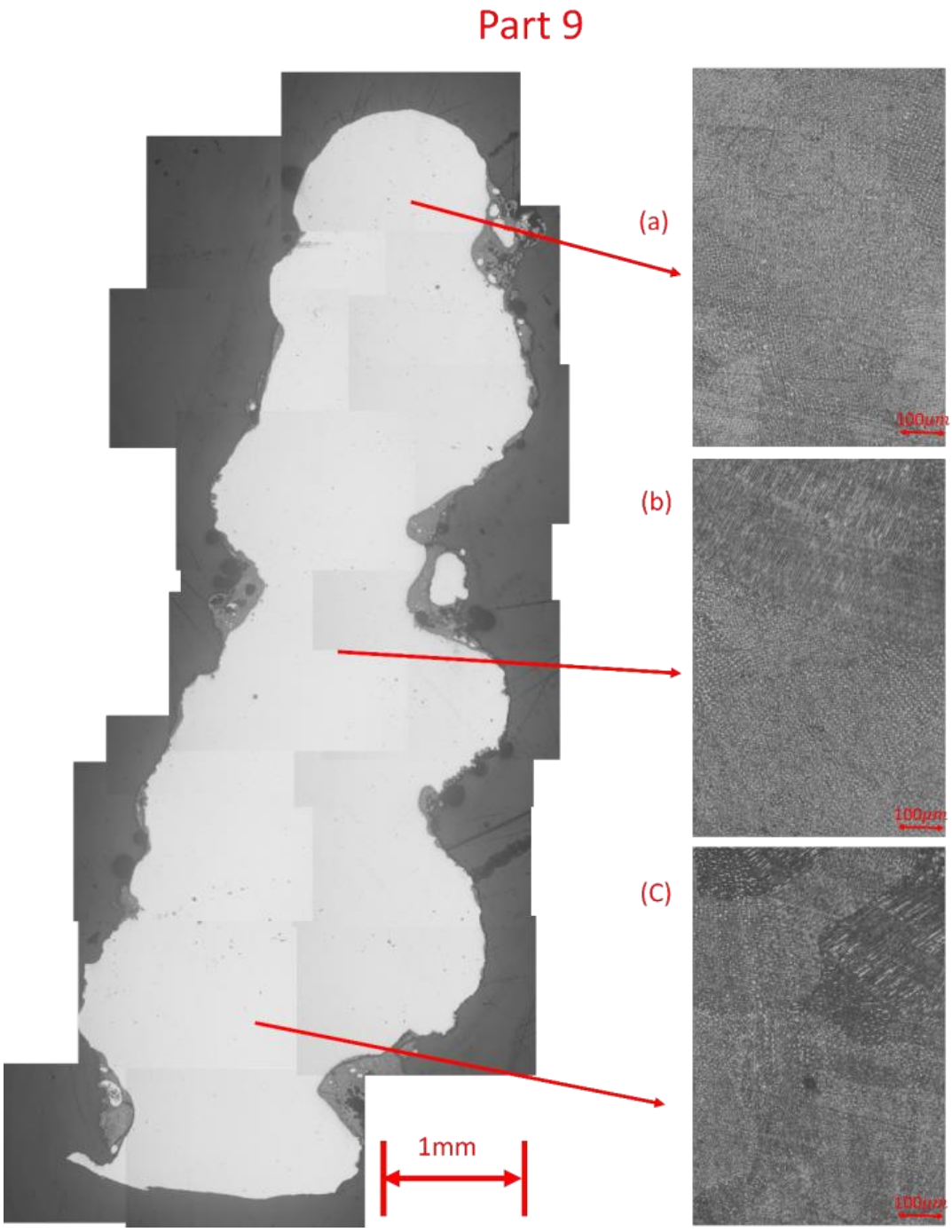

Figure 4.21 Microscopic image of sample 9: The figure on the left is the microscopic image before etching. The gray region is the sample. Images a-c are images after etching. Image (a) was taken from the top of the sample, image (b) from the center of the sample, and image (b) from the bottom of the sample.

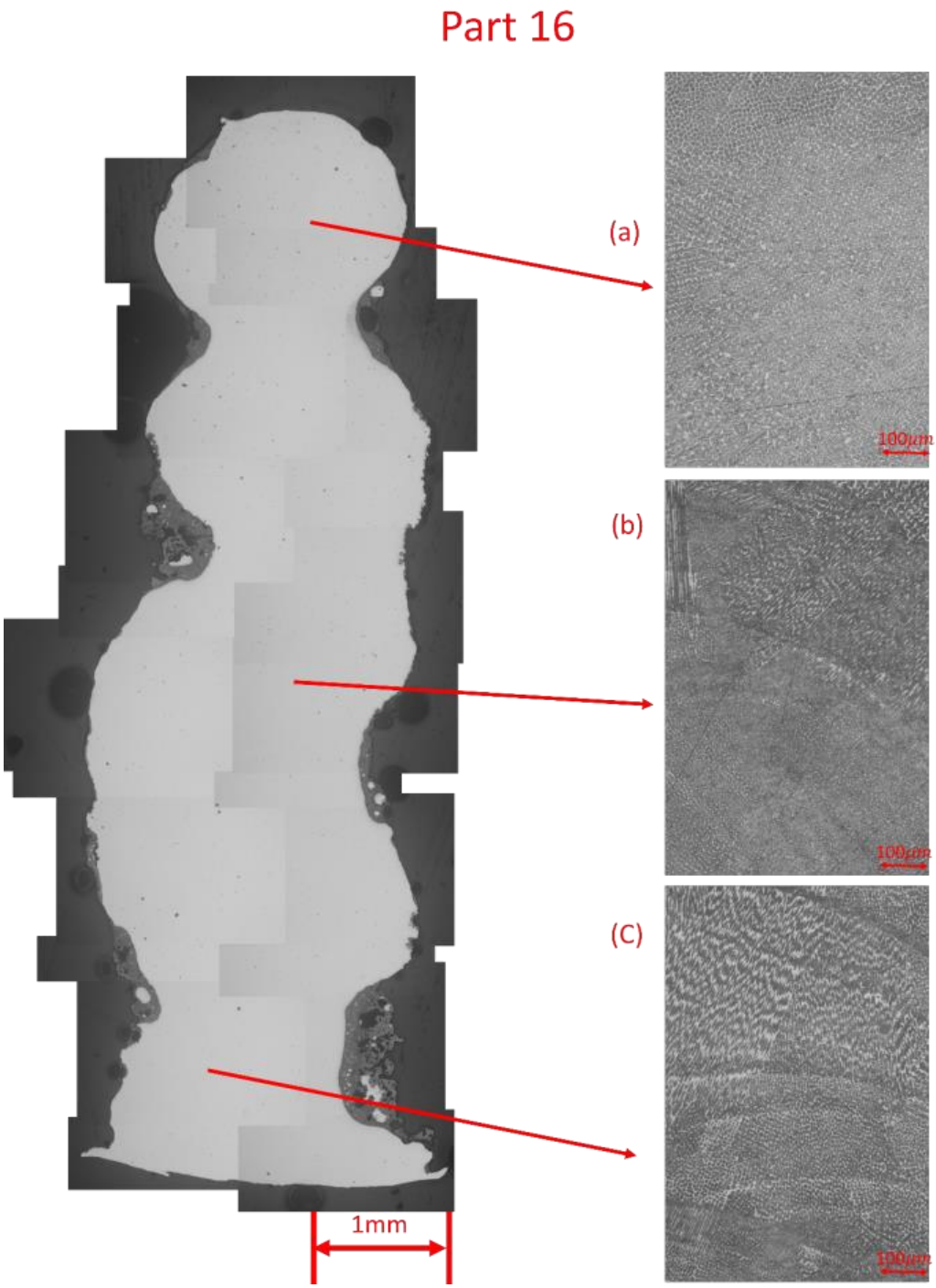

Figure 4.22 Microscopic image of sample 16: The figure on the left is the microscopic image before etching. The gray region is the sample. Images a-c are images after etching. Image (a) was taken from the top of the sample, image (b) from the center of the sample, and image (b) from the bottom of the sample.

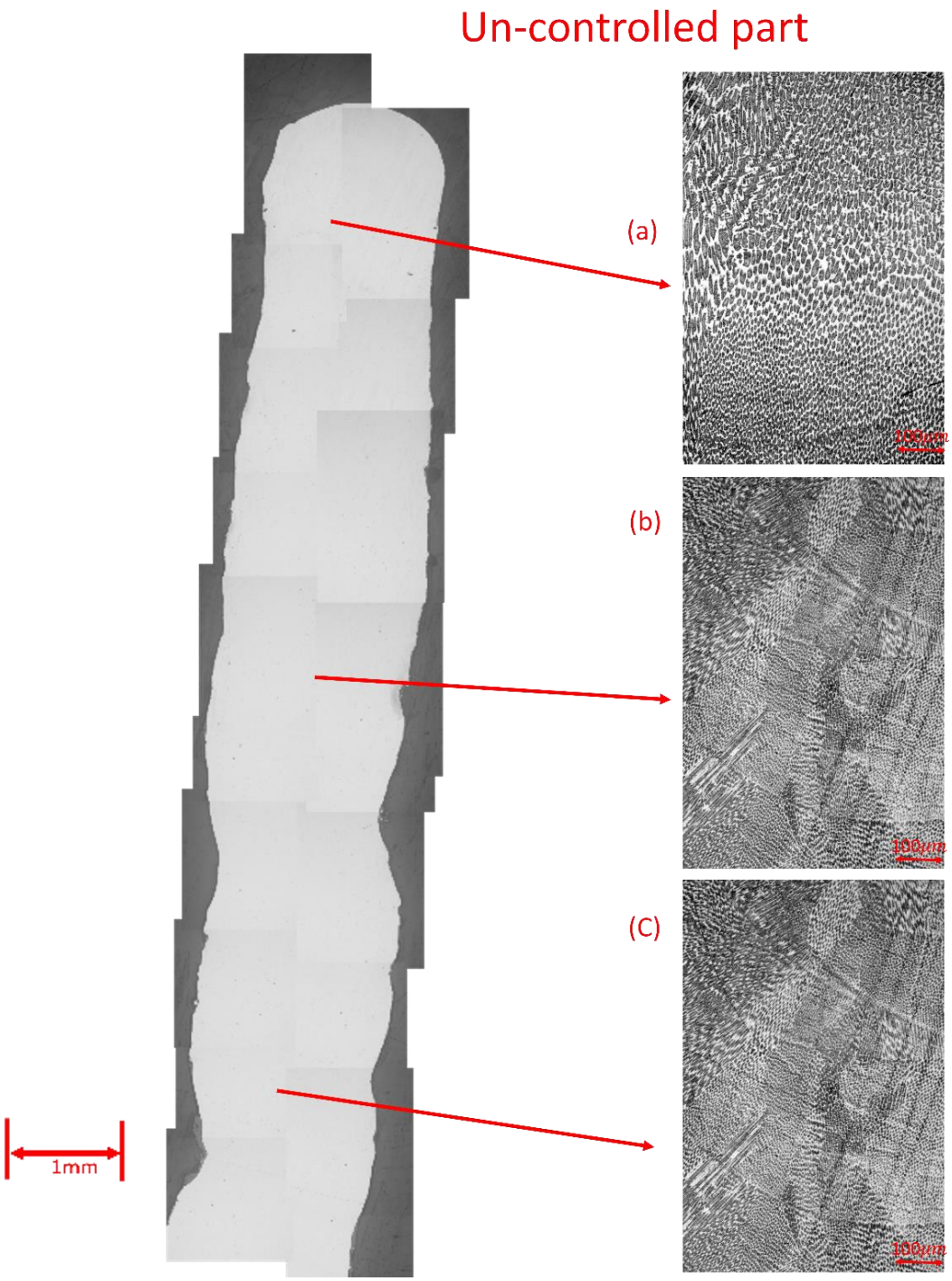

Figure 4.23 Microscopic image of the uncontrolled part: The figure on the left is the microscopic image before etching. The gray region is the sample. Images a-c are images after etching. Image (a) was taken from the top of the sample, image (b) from the center of the sample, and image (b) from the bottom of the sample.

Table 4.4 Maximum pore diameter of parts

Part #		Top	Center	Bottom
		Maximum pore diameter (mm)	Maximum pore diameter (mm)	Maximum pore diameter (mm)
Uncontrolled part		0.006	0.006	0.004
Thin parts	Part 5	0.021	0.014	0.004
	Part 15	0.012	0.005	0.004
Thick parts	Part 9	0.015	0.007	0.015
	Part 16	0.018	0.026	0.026

4.4 FUTURE IMPLEMENTATION

The control system used a method similar to a go/no-go method. When the building speed became too fast, with even the linear table running at the set max table speed, the top of the part eventually will become much higher than the pyrometer's aiming position. In this situation, readings from the pyrometer will never reach the set control temperature. Therefore, the system will keep depositing material on the same point until the part is too high and it hits the powder feeding tube.

In such a scenario, a setup can be implemented to improve the height control system and resolve the situation. Figure 4.24 is the schematic diagram of the improved height monitoring device.

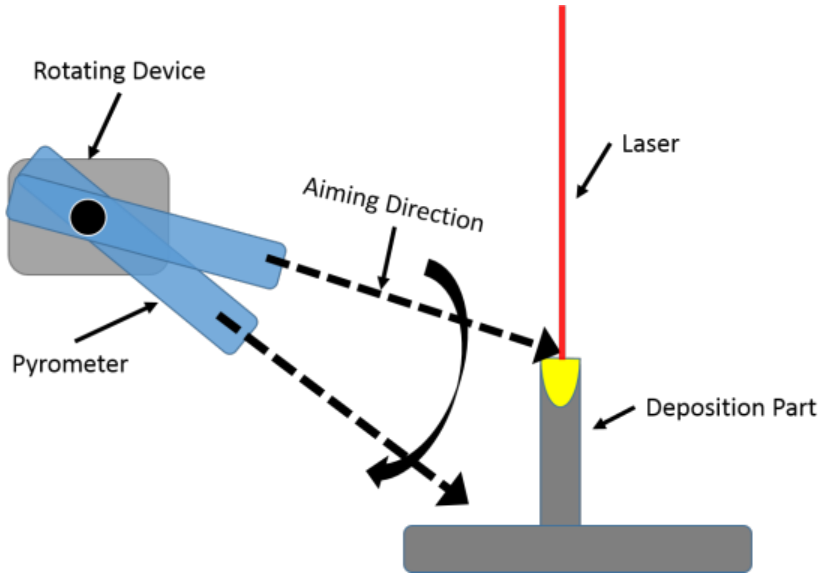

Figure 4.24 Proposed new height monitoring device. This system mounts a pyrometer on a rotating device to scan the temperature across the part.

As Figure 4.24 shows, this proposed setup uses a rotating device. The pyrometer moves along on the part, supplying the control system with complete temperature information from the part surface. The system also can recognize the height of the part by analyzing the position with the highest temperature. As long as the rotation speed and the data acquisition rate of the pyrometer are fast enough (faster than 1k Hz), this system should have more stable performance than systems currently in use.

5. CONCLUSION

A height control system for the LMD process was designed and tested. Tests were conducted to determine the system's accuracy, repeatability, and properties under different settings. Part samples were examined microscopically to ensure that the system did not increase the porosity of the built parts. The highlights of the study were as follows:

- An LMD height control system was developed.
- An LMD system with height control can build parts with parameters that normally cause uncontrolled systems to fail.
- A simulation of the effect of powder stream misalignment on the powder capturing rate was performed.
- The height repeatability and accuracy of the system was measured:
    - Height repeatability : +-0.47 mm
    - Height accuracy: +- 1.02 mm
- A higher powder flow rate and layer thickness can increase the material efficiency of the process.
- A lower laser power setpoint, lower layer thickness, and higher powder feed rate increase the part height build rate.
- A higher laser power setpoint, layer thickness, and powder feed rate increase the part volume build rate.
- A lower laser power setpoint and layer thickness can decrease a part's surface roughness.

- The height control system may produce parts with larger pores than uncontrolled systems.

5.1 SUGGESTED RESEARCH

- Integrating table motion monitoring sensors with the height control system is essential to determine the effect of table motion on surface roughness and part porosity.
- Current knowledge available about the influence of powder properties (e.g. material, mesh size, powder shape, etc.) on the height control system is insufficient. Testing part porosity and surface roughness values of multiple powder material systems will lead to the accumulation of valuable research data.
- Increasing the resolution and accuracy of the height control system by using pyrometers and similar sensors with shorter settling time and smaller measuring area.

REFERENCES

[1] J. Ruan, T. E. Sparks, Z. Fan, J. K. Stroble, A. Panackal, F. Liou, "A Review of Layer Based Manufacturing Processes for Metals," Department of Mechanical and Aerospace Engineering, Missouri University of Science and Technology (formerly University of Missouri – Rolla), Proceedings of the 17th Annual SFF Symposium, Austin, TX, pp. 233-245 (2006).

[2] Choi, j.," Process and Properties Control in Laser Aided Direct Metal/Materials Deposition Process," Proceedings of IMECE, New Orleans, LA, November 17-22, pp. 1-9 (2002).

[3] Yaxin Bao, "Mechanical Properties and Microstructure Study for Direct Metal Deposition of Titanium Alloy and Tool Steel," A Thesis, Missouri University of Science and Technology (formerly University of Missouri-Rolla) (2007).

[4] Patrick Sammons,"Height Dependent Laser Metal Deposition Process Modeling," A Thesis, Missouri University of Science and Technology (formerly University of Missouri-Rolla) (2012).

[5] E. Fearon, K. G. Watkins, "Optimal of Layer Thickness Control in Direct Laser Deposition," Proceedings of the 23rd International Congress on Applications of Lasers and Electro-Optics, San Francisco, California, October 4-7,pp. 1708 (2004).

[6] Lie Tang, "Variable Powder Flow Rate Control in Laser Metal Deposition Process," A Thesis, Missouri University of Science and Technology (formerly University of Missouri-Rolla) (2007).

[7] G. Muscato, G. Spampinato, L. Cantelli, "A Closed Loop Welding Controller for a Rapid Manufacturing Process," Process Emerging Technologies and Factory Automation. ETFA 2008. IEEE International Conference, pp. 1080-1083 (2008).

[8] L. Song, V. Bagavath, B. Dutta, J. Mazumder, "Control of Melt Pool Temperature and Deposition Height During Direct Metal Deposition Process," International Journal of Advance Manufacturing Technology, Vol. 58, pp. 247–256 (2012).

[9] R. Barclay, "Parameter Optimization for Controlling Aluminum Loss When Laser Depositing Ti-6Al-4V," A Thesis, Missouri University of Science and Technology (formerly University of Missouri-Rolla) (2013).

[10] S. Dongare, “Development of a Technique for Testing of Tensile Properties with Miniature Size Specimens for Metal Additive Manufacturing,” A Thesis, Missouri University of Science and Technology (formerly University of Missouri-Rolla) (2012).

VITA

The author, Yu_Herng Pan, son of Ci_Ling Pan and Ru_Ping Chao, was born in Taipei, Taiwan, in 1984. He successfully completed his studies and earned his bachelor's degree from the National Cheng Kung University in August 2008. After a year of mandatory military service, he worked as a research assistant at the National Cheng Kung University.

In January 2011, he joined the Missouri University of Science and Technology (Missouri S&T) to pursue his Master's in Manufacturing Engineering. He was granted the position of Graduate Research Assistant in the Laser Aided Manufacturing Processes Lab at Missouri S&T. His research focused primarily on manufacturing techniques for direct laser metal deposition. Yu_Herng Pan was awarded the M.S. in Manufacturing Engineering in August 2013.